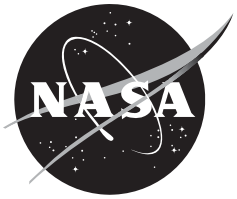
NASA/TM—2013–216620



Mars Sample Return: Mars Ascent Vehicle Mission & Technology Requirements

Jeffrey V. Bowles
Systems Analysis and Integration Branch
Ames Research Center, Moffett Field, California

Loc C. Huynh
Science and Technology Corporation, Hampton, VA

Veronica M. Hawke
Science and Technology Corporation, Hampton, VA

Xun J. Jiang
Science and Technology Corporation, Hampton, VA

November 2013

NASA STI Program ... in Profile

Since its founding, NASA has been dedicated to the advancement of aeronautics and space science. The NASA scientific and technical information (STI) program plays a key part in helping NASA maintain this important role.

The NASA STI program operates under the auspices of the Agency Chief Information Officer. It collects, organizes, provides for archiving, and disseminates NASA's STI. The NASA STI program provides access to the NASA Aeronautics and Space Database and its public interface, the NASA Technical Reports Server, thus providing one of the largest collections of aeronautical and space science STI in the world. Results are published in both non-NASA channels and by NASA in the NASA STI Report Series, which includes the following report types:

- TECHNICAL PUBLICATION. Reports of completed research or a major significant phase of research that present the results of NASA Programs and include extensive data or theoretical analysis. Includes compilations of significant scientific and technical data and information deemed to be of continuing reference value. NASA counterpart of peer-reviewed formal professional papers but has less stringent limitations on manuscript length and extent of graphic presentations.

- TECHNICAL MEMORANDUM. Scientific and technical findings that are preliminary or of specialized interest, e.g., quick release reports, working papers, and bibliographies that contain minimal annotation. Does not contain extensive analysis.

- CONTRACTOR REPORT. Scientific and technical findings by NASA-sponsored contractors and grantees.

- CONFERENCE PUBLICATION. Collected papers from scientific and technical conferences, symposia, seminars, or other meetings sponsored or co-sponsored by NASA.

- SPECIAL PUBLICATION. Scientific, technical, or historical information from NASA programs, projects, and missions, often concerned with subjects having substantial public interest.

- TECHNICAL TRANSLATION. English-language translations of foreign scientific and technical material pertinent to NASA's mission.

Specialized services also include organizing and publishing research results, distributing specialized research announcements and feeds, providing information desk and personal search support, and enabling data exchange services.

For more information about the NASA STI program, see the following:

- Access the NASA STI program home page at http://www.sti.nasa.gov

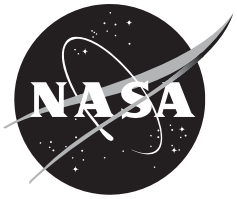
- E-mail your question to help@sti.nasa.gov

- Fax your question to the NASA STI Information Desk at 443-757-5803

- Phone the NASA STI Information Desk at 443-757-5802

- Write to:
  STI Information Desk
  NASA Center for AeroSpace Information
  7115 Standard Drive
  Hanover, MD 21076-1320

NASA/TM—2013–216620



Mars Sample Return: Mars Ascent Vehicle Mission & Technology Requirements

Jeffrey V. Bowles
Systems Analysis and Integration Branch
Ames Research Center, Moffett Field, California

Loc C. Huynh
Science and Technology Corporation, Hampton, VA

Veronica M. Hawke
Science and Technology Corporation, Hampton, VA

Xun J. Jiang
Science and Technology Corporation, Hampton, VA

National Aeronautics and
Space Administration

Ames Research Center
Moffett Field, CA 94035-1000

November 2013

Acknowledgments

This work was performed by the AUS (Systems Analysis and Integration) Branch at NASA Ames in conjunction with AEMMS contract NNA10DF25C with Science and Technology Corporation.

Available from:

NASA Center for AeroSpace Information
7115 Standard Drive
Hanover, MD 21076-1320
443-757-5802

This report is also available in electronic form at

http://

Table of Contents

1.0 Introduction 4
2.0 Objective and Technical Approach 4
3.0 Mission Requirements 4
4.0 Assumptions and Ground Rules 5
5.0 Initial Baseline Configuration Selection 6
5.1 Baseline Engine 6
5.2 Candidate Body Geometries 8
5.3 Aerodynamics & Aerothermodynamics 10
5.4 General Arrangement and Tank Configuration 13
5.5 Mass Estimating Relationships 15
6.0 Trajectory 16
7.0 Baseline Configurations 21
7.1 Vehicle Closure 21
7.2 Orbital Architecture 21
7.3 C_3=0 Architecture 23
8.0 Trade Studies 25
8.1 Number of Engines 26
8.2 Pressure-Feed Propulsion System 27
8.3 Cryogenic Propellant Trade 32
9.0 Final Configurations 38
9.1 Inert Capsule to low Mars orbit rendezvous 38
9.2 Optimized ΔV Split Architecture 38
9.3 SEP Architecture 39
10.0 Conclusions & Recommendations 40
Appendix A: Engine Trades 42
Appendix B: Propellant Trades 46
Appendix C: CFD Solutions & Aeroheating 48
References 54

Table of Figures

Figure 5.1.1 Burn-out mass fraction versus engine specific impulse 7
Figure 5.1.2 Propellant fraction and overall body length versus engine expansion ratio 7
Figure 5.1.3 Gross liftoff mass and dry mass versus engine expansion ratio 8
Figure 5.2.1 Parametric body shapes 9
Figure 5.2.2 Overall vehicle length and total wetted area versus body fineness ratio 9
Figure 5.2.3 Overall vehicle length and total wetted area versus body fineness ratio 10
Figure 5.3.1 Drag coefficient versus angle-of-attack and Mach number 11
Figure 5.3.2 CBAero predicted zero-lift drag coefficient versus Mach number and free stream dynamic pressure 12
Figure 5.3.3 CBAero predicted drag coefficient versus angle-of-attack and Mach number for dynamic pressure = 0.005 bars 12
Figure 5.3.4 CBAero predicted lift coefficient versus angle-of-attack and Mach number for dynamic pressure = 0.005 bars 13
Figure 5.4.1 MAV general arrangement 14
Figure 5.4.2 MAV internal arrangement 14
Figure 5.5.1 Inter-tank and aft compartment structure mass estimate model (taken from Reference 5) 15
Figure 5.5.2 Rocket engine weight-to-thrust ratio versus engine thrust 16
Figure 6.1 MAV ascent trajectory: Altitude versus time 17
Figure 6.2 MAV ascent trajectory: Altitude versus relative velocity 18
Figure 6.3 MAV ascent trajectory: Dynamic pressure versus time 18
Figure 6.4 MAV ascent trajectory: Acceleration versus time 19
Figure 6.5 MAV ascent trajectory: Dynamic pressure versus relative velocity 19
Figure 6.6 Orbital relative velocity loss breakdown 20
Figure 6.7 Escape relative velocity loss breakdown 20
Figure 7.2.1 Orbital architecture closure point versus GLOM and payload mass 22
Figure 7.2.2 Orbital Architecture, 200 kg payload MAV dimensions 23
Figure 7.3.1 C_3=0 architecture closure mass versus GLOM and payload mass 24
Figure 7.3.2 C3=0, 120 kg payload MAV dimensions 25
Figure 8.2.1 Propellant fraction required versus chamber pressure 28
Figure 8.2.2 Overall vehicle length versus chamber pressure 28
Figure 8.2.3 Tank, pressurization and engine mass versus chamber pressure 29
Figure 8.2.4 GLOW and dry mass versus chamber pressure 29
Figure 8.2.5 GLOW and dry mass versus chamber pressure 30
Figure 8.2.6 Vehicle overall versus chamber pressure 31
Figure 8.3.1 Relative gross liftoff mass versus relative engine specific impulse 35
Figure 8.3.2 Relative dry mass versus relative engine specific impulse 36
Figure 8.3.3 Relative vehicle length versus relative engine specific impulse 36
Figure 8.3.4 Relative gross liftoff mass versus relative engine mass 37
Figure 8.3.5 Relative dry mass versus relative engine mass 37
Figure 8.3.6 Relative overall vehicle length versus relative engine specific mass 38
Figure A1. Engine specific impulse versus chamber pressure and nozzle expansion ratio. 43
Figure A2. Engine thrust per unit nozzle exit area versus chamber pressure and nozzle expansion ratio 43
Figure A3. Engine mass versus chamber pressure and nozzle expansion ratio. 44
Figure A4. Engine diameter versus chamber pressure and nozzle expansion ratio. 44
Figure A5. Engine thrust-to-weight versus chamber pressure and nozzle expansion ratio. 45
Figure B1. Engine specific impulse versus nozzle expansion ratio for various hypergolic fuels with NTO. 46
Figure B2. Engine specific impulse versus nozzle expansion ratio for various hydrocarbon fuels with liquid oxygen 47
Figure C1. Cart3D predicted subsonic Mach = 0.6 surface pressure distribution for the Rev0 geometry 49

Figure C2. Cart3D predicted subsonic Mach = 0.5 surface pressure distribution and Mach number contours for the Rev2 geometry 49
Figure C3. Cart3D predicted Mach = 0.95 surface pressure distribution and Mach number contours for the Rev2 geometry 50
Figure C4. Cart3D predicted Mach = 2.0 surface pressure distribution and Mach number contours for the Rev2 geometry 50
Figure C5. Cart3D predicted Mach = 2.0 and angle-of-attack = 10.0° surface pressure distribution and Mach number contours for the Rev2 geometry 51
Figure C6. Zero-lift drag coefficient versus Mach number computed by CFD Euler code 51
Figure C7. Cart3D predicted pitching moment coefficient versus angle-of-attack and Mach number contours for the Rev2 geometry 52
Figure C8. Mission maximum convective heating distribution for Rev2 geometry 52
Figure C9. Mission integrated heat load for Rev2 geometry 53

Table of Tables

Table 1 Ascent Velocities and mass fractions 17
Table 2. Orbital architecture characteristics 23
Table 3. Escape architecture characteristics 25
Table 4 Number of Engine comparison 26
Table 5. 20kg payload pump feed versus pressure feed system comparison 30
Table 6. 200 kg Payload mass pump feed versus pressure feed system comparison 31
Table 7. Propellant properties 33
Table 8. Orbital/200kg payload hypergolic and cryogenic performance comparison 34
Table 9. Orbital/200kg comparison between hypergolic and cryogenic propellants 34
Table 10. C3=0/120kg comparison between hypergolic and cryogenic propellants 35
Table 11. Final concepts mass statement and dimensions 40

Revision History

Original Release	March 2013	NASA/TM-2013-216511
RevA	November 2013	

1.0 Introduction

A Mars Sample Return (MSR) mission is the highest priority science mission for the next decade recommended by the recent Decadal Survey of Planetary Science, the key community input process that guides NASA's science missions. A feasibility study was conducted of a potentially simple and low cost approach to Mars Sample Return mission enabled by the use of developing commercial capabilities. Previous studies of MSR have shown that landing an all up sample return mission with a high mass capacity lander is a cost effective approach. The approach proposed is the use of an emerging commercially available capsule to land the launch vehicle system that would return samples to Earth. This paper describes the mission and technology requirements impact on the launch vehicle system design, referred to as the Mars Ascent Vehicle (MAV).

2.0 Objective and Technical Approach

The objective of this study is to determine the mission and technology requirements impact on the MAV design by performing a conceptual design of several candidate configurations to establish baseline designs, and then executing sensitivity and technology trade studies on these baseline concepts. A set of mass estimating relationships (MERs) at the subsystem level were developed for this class of vehicle, and integrated into a vehicle synthesis code for computing mass and volume, and performing vehicle closure to meet mission requirements. These MERs included the expected elements such as structures, power system, propulsion system, nose fairing, thermal insulation, actuation devices, guidance and communication.

A parametric set of candidate outer mold-line (OML) configurations were defined and associated geometric characteristics determined. Aero and aero-thermal databases were developed for each OML configuration. Preliminary selection of the propulsion system was selected and initial trajectory optimization preformed to establish total ΔV requirements.

Baseline deigns were established for two Mars Sample Return architectural approaches: launching an inert or powered Earth Return Vehicle (ERV) to low Mars orbit, and launching a powered ERV to escape velocity, with the ERV providing the remaining ΔV for trans-earth injection/capture. With these baseline designs determined, trade studies on mission requirements and alternate technology approaches were performed.

3.0 Mission Requirements

The mass and volume available for the launch stack (MAV and ERV) contained within a landing capsule depends on the possible mass/volume that can be landed. Preliminary analysis has indicated that a capsule could land up to 2+ mT at terrain elevations between -1 and +1.6 km elevation. Open literature diagrams of a representative capsule show that the central internal volume is approximately 1.2 m diameter and 4+ m length. The landed mass and size provide boundary conditions for the other elements of the study, and impose unique requirements and considerations on the MAV design

The Mars Ascent vehicle (first stage) was designed for an assumed single stage to orbit or escape C3=0 or points in-between. The launch point was 0m MOLA altitude, 0º Latitude and 0º Longitude, heading due East. A 5% reserve for ascent propellants was assumed.

Payload volume was based on an assumed payload density, which in turn was a function of the type of ERV propulsion concept. The MAV was sized to provide sufficient internal volume to

accommodate propellants and payload volume, with an assumed packing efficiency to provide sufficient internal volume of other subsystems.

4.0 Assumptions and Ground Rules

The MAV was sized for each value of total ΔV and assumed payload mass using a set of assumptions and ground rules. These assumptions are based on best practices and experience for the conceptual design phase.

Load bearing structures, including forward and aft compartments, and inter-tank were assumed to be high temperature thermo-plastic composites, skin-stringer stiffened semi-moncoque construction. A design load of 5.0 axial Earth g's (launch from Earth) was used to size the load bearing structure, with a safety factor of 1.4 on loads and a knock-down factor of 0.80 on stiffness. Non-load bearing aeroshell structure was assumed to be min-gauge (5 plies) thermo-plastic. Secondary structure was assumed to be 10% of primary structure.

Propellant tanks were also assumed to be high temperature thermo-plastic composites with a liner, and were sized using historical weight trends. A 20% reduction in tank mass was used to account for composite construction, as opposed to metal tanks used in the historical correlation for tank weights. A factor of safety of 2.0 was used for tank internal pressure. A 5% ullage volume was assumed for all propellant tanks. For hypergolic propellants, a low ullage pressure of .0345 MPa (5 psig) was used, while for cryogenic tanks a tank pressure of 0.172 MPa (25 psig) was assumed. For pressure feed propellant systems, tank pressure was 25% higher than the thrust chamber pressure to account for total pressure losses the feed system. Because of low tank pressure, hypergolic tanks were assumed to have a dome eccentricity of 0.90 (relatively "flat" domes) to improve overall vehicle packing efficiency, while higher pressure tanks (cryogenic propellants and pressure-feed systems) used a tank dome eccentricity of 0.707.

Because of the relatively benign aeroheating environments for Mars launch, minimum gauge P-45 cork was applied to the spherical nose cap region for thermal protection. Base closeout TPS consisted of 0.25 inches of P-45 cork. Cryogenic tank insulation was assumed to be light-weight closed-cell foam and was sized to provide 15 minute pre-launch hold time to prevent CO_2 condensation on the tank exterior walls.

Rocket engine performance was computed assuming chemical equilibrium in the combustor and up to the nozzle throat. Downstream of the throat, the nozzle flow was assumed to be chemically frozen (i.e. combustion product constituent mole fractions fixed at the throat values). Propellant initial temperature was assumed to be -10°C for hypergolic propellants and at normal boiling point for cryogenic propellants. Based on preliminary ascent trajectory optimizations, a liftoff thrust-to-weight ratio of 2.5 was used. Propellant oxidizer-to-fuel ratio was optimized for maximum engine specific impulse and nozzle expansion ratio for minimum launch mass. Startup propellant was computed assuming 2.0 seconds of engine ignition time.

Lithium-ion batteries were used for prime power and assumed power density of 0.056 watts per pound with a 20% power margin applied. Five controller functions were used at 0.1kW per channel. A total ascent time of 300 seconds was used to size battery mass. Controller mass was assumed to be 0.45 kg (1.0 lb) each. Engine thrust vector control was achieved using a pressurized helium pneumatic system. For DHCC, a total mass allocation of 1.0 kg was assumed, while GN&C and Data Processing system mass was charged to the ERV. A weight growth allowance of 30% was used for all dry mass elements.

5.0 Initial Baseline Configuration Selection

As a starting point, an initial design was selected as the baseline vehicle, including engine type, propellant selection, structural arrangement and outer mold line configuration. In anticipation of overall vehicle length constraints imposed by the landing capsule, a single stage-to-orbit architecture was selected. Integration of multi-stage configuration into a single stack could result in increased overall vehicle length even with the benefit of reduced total ascent propellant mass fraction.

5.1 Baseline Engine

The significance of a high performance rocket engine is demonstrated in Figure 5.1.1, where the burn-out mass fraction (essentially the vehicle dry mass plus payload) is plotted versus engine specific impulse for two ascent total required delta-V, orbital at 4150 m/sec and escape C3=0 at 5500 m/sec. As engine specific impulse is increased, the mass fraction for dry mass and payload increase. The higher the required total delta-V, the higher the propellant mass fraction, hence lower payload plus dry mass fraction. For the C3=0 case in particular, specific impulse on the order of roughly 340 seconds allows for achievable mass fractions on the order of 20%, hence reasonable payload mass fractions.

Based on the requirement for relatively high engine specific impulse and the consideration of single-stage-to-orbit dictated by overall vehicle length constraints, a hypergolic, pressure-feed, gas-generator cycle engine was selected as the baseline concept. As a reference engine, the XLR-132 engine was selected, with an engine specific impulse of 347 seconds, combustor pressure of 10.34 MPa (1500 psi) and an engine thrust-to-weight ratio of approximately 33. During the vehicle sizing process, the engine was scaled up or down to match the required lift-off vehicle thrust-to-weight ratio.

An initial engine trade study was conducted to assess the impact of the overall nozzle expansion ratio on the vehicle closure mass. As the expansion ratio is increased, the engine performance as measured by specific impulse increases, however the nozzle becomes larger and the engine weight increases. In addition for this particular application, the higher expansion ratio results in a longer engine length, and hence potentially a longer over vehicle length, perhaps being constrained by the overall vehicle length limits imposed by the landing capsule. Upper limits on nozzle expansion ratio were imposed to prevent an over expanded nozzle on the surface of Mars. Appendix A presents impact of nozzle expansion ratio on engine performance characteristics, dimensions and weight.

Figure 5.1.2 presents the propellant mass fraction and overall body length as a function of engine expansion ratio for a delta-V requirement of 4150 m/sec and a payload mass of 200 kg. As the expansion ratio is increased, the engine specific impulse increases due to more optimal nozzle performance resulting in lower required propellant fraction, while overall closed vehicle length also increases due to increased nozzle length. The resultant closed vehicle gross liftoff mass and vehicle dry mass is presented in Figure 5.1.3 as a function of engine nozzle expansion ratio. As the nozzle expansion ratio is increased, the vehicle dry mass also increases due to heavier engine mass associated with a larger nozzle. However there is a minimum in the gross liftoff mass with expansion ratio, with higher propellant mass and lower dry mass for lower expansion ratios versus reduced propellant mass and increased dry mass at higher expansion ratios. The overall trend in gross liftoff mass is fairly flat, with roughly a 1.5 % variation over the range of nozzle expansion ratios analyzed. If the overall vehicle length becomes a constraint, only a modest penalty in gross liftoff mass will occur.

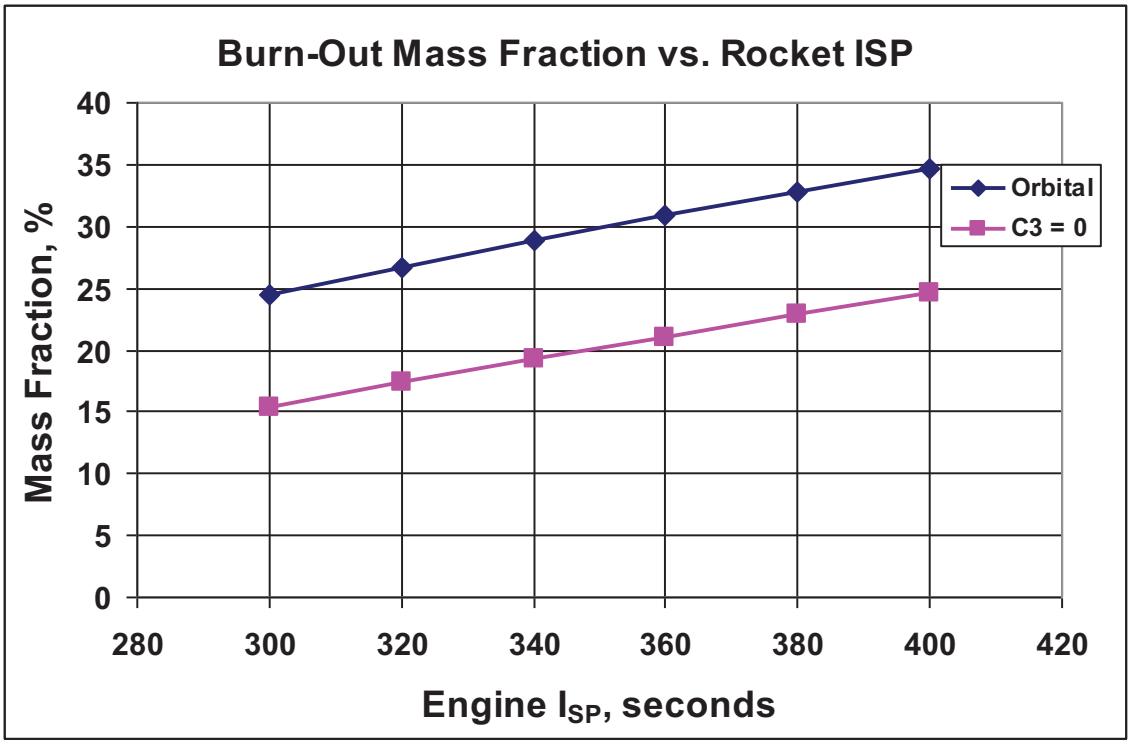


Figure 5.1.1 Burn-out mass fraction versus engine specific impulse

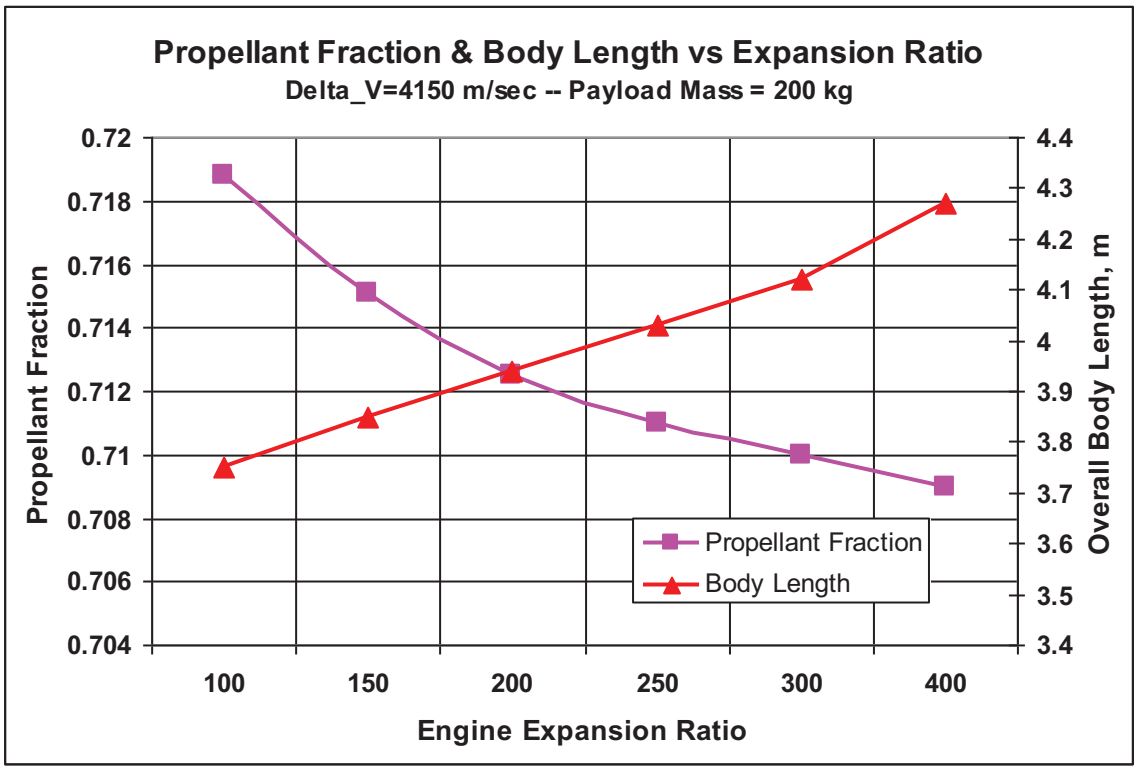


Figure 5.1.2 Propellant fraction and overall body length versus engine expansion ratio

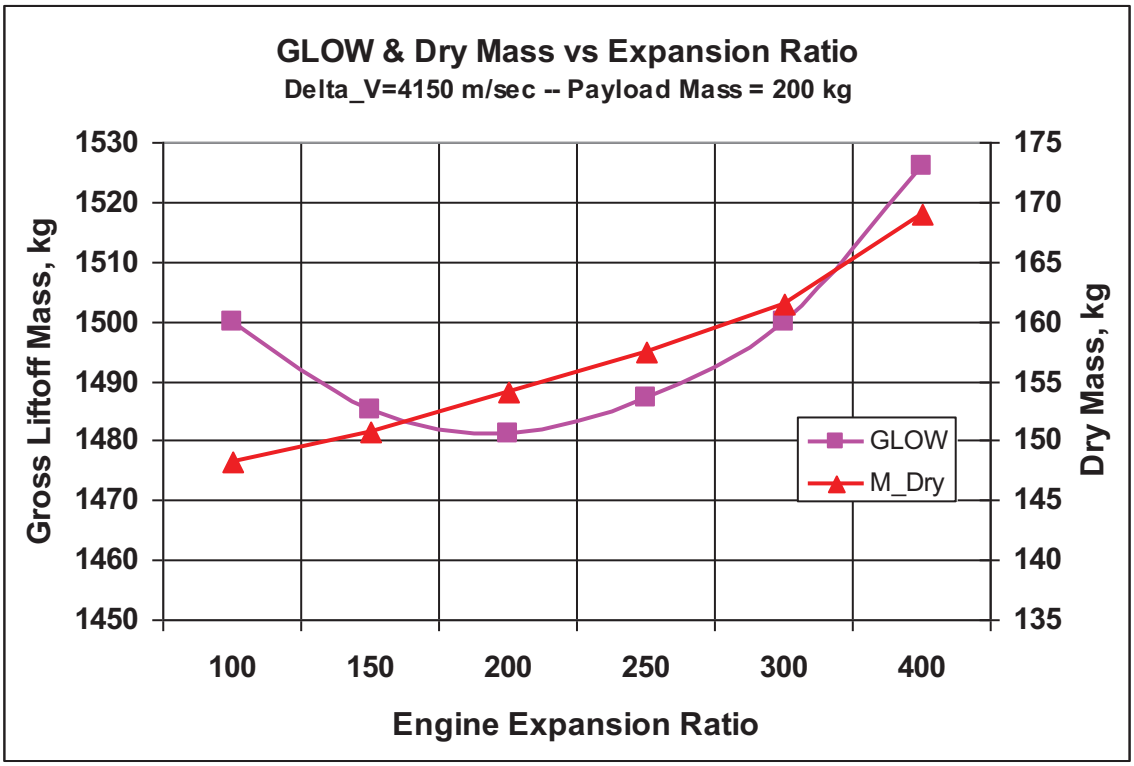


Figure 5.1.3 Gross liftoff mass and dry mass versus engine expansion ratio

5.2 Candidate Body Geometries

In order to define the design space for the general configuration of the MAV, three fore body shapes were selected, with the body fineness ratio (defined as body diameter divided by body length) varied parametrically from a range of approximately 0.2 to 0.44, and are presented in Figure 5.2.1. For each shape, a surface grid was generated, consisting of a triangulated mesh ranging for roughly 5,000 to 15,000 triangles. Body diameter, wetted area and internal volume as a function of axial coordinate were computed and used in the vehicle sizing code closure process.

An initial trade study was conducted to assess the impact of body fineness ratio on closed vehicle mass and dimensions. For a delta-V requirement of 4150 m/sec and a payload mass of 200 kg, Figure 5.2.2 presents sized vehicle overall length and surface wetted area as a function of body fineness ratio. As the fineness ratio is increased, both closed vehicle length and wetted area decrease. The variation in closed gross liftoff mass and vehicle dry mass are shown in Figure 5.2.3, with a general trend in lower gross and dry mass with increasing fineness ratio. Meeting the possible constraint on overall vehicle length can be addressed by going to a lower fineness ratio with only small impacts on gross liftoff and vehicle dry mass.

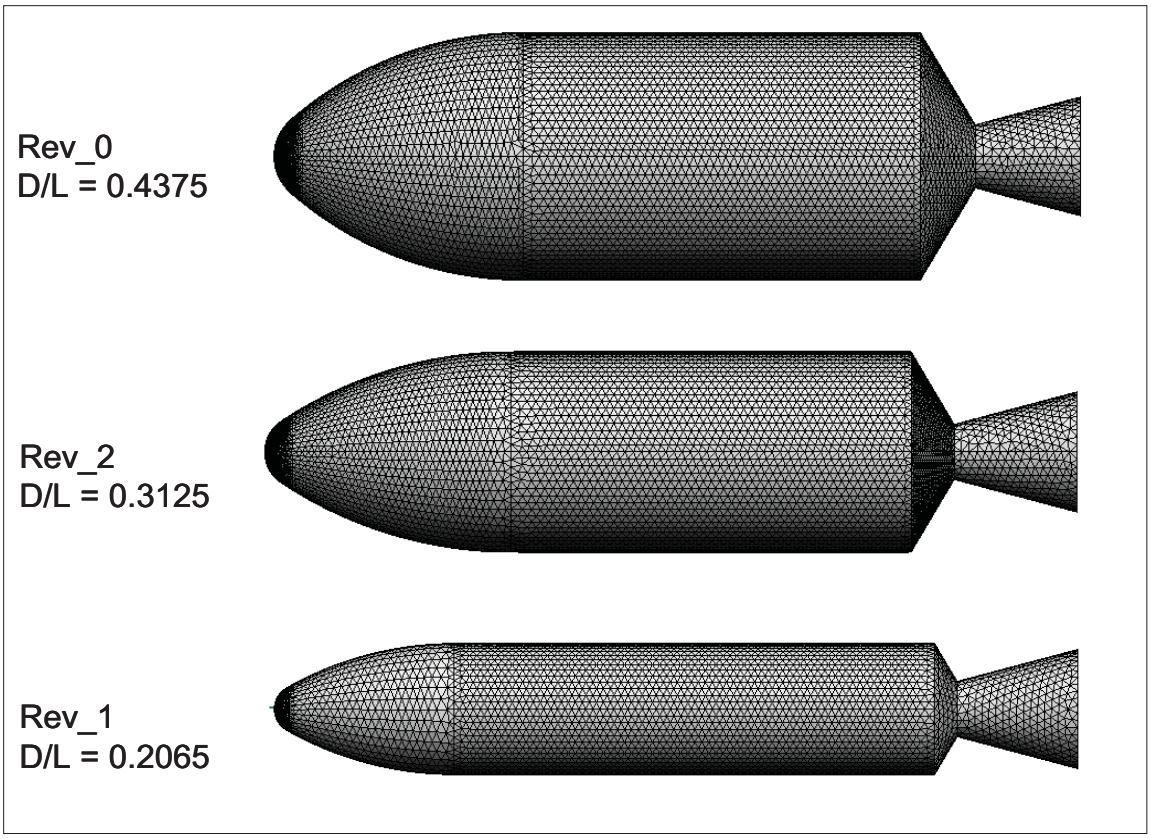


Figure 5.2.1 Parametric body shapes

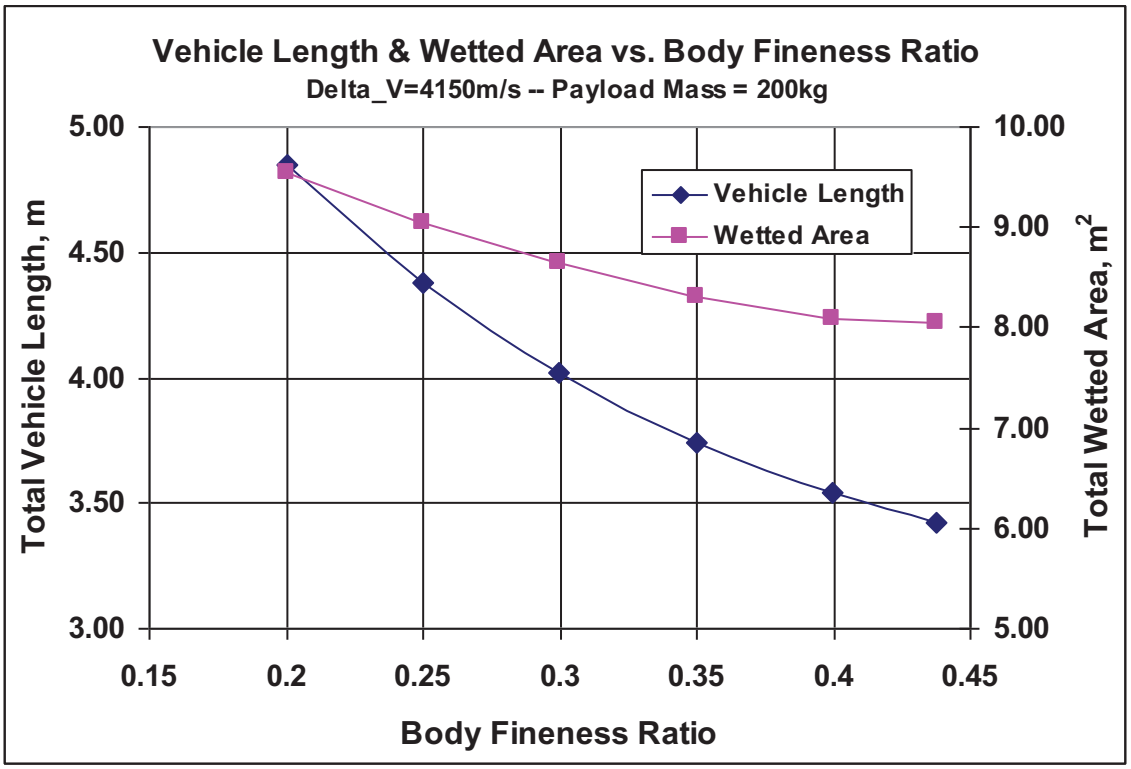


Figure 5.2.2 Overall vehicle length and total wetted area versus body fineness ratio

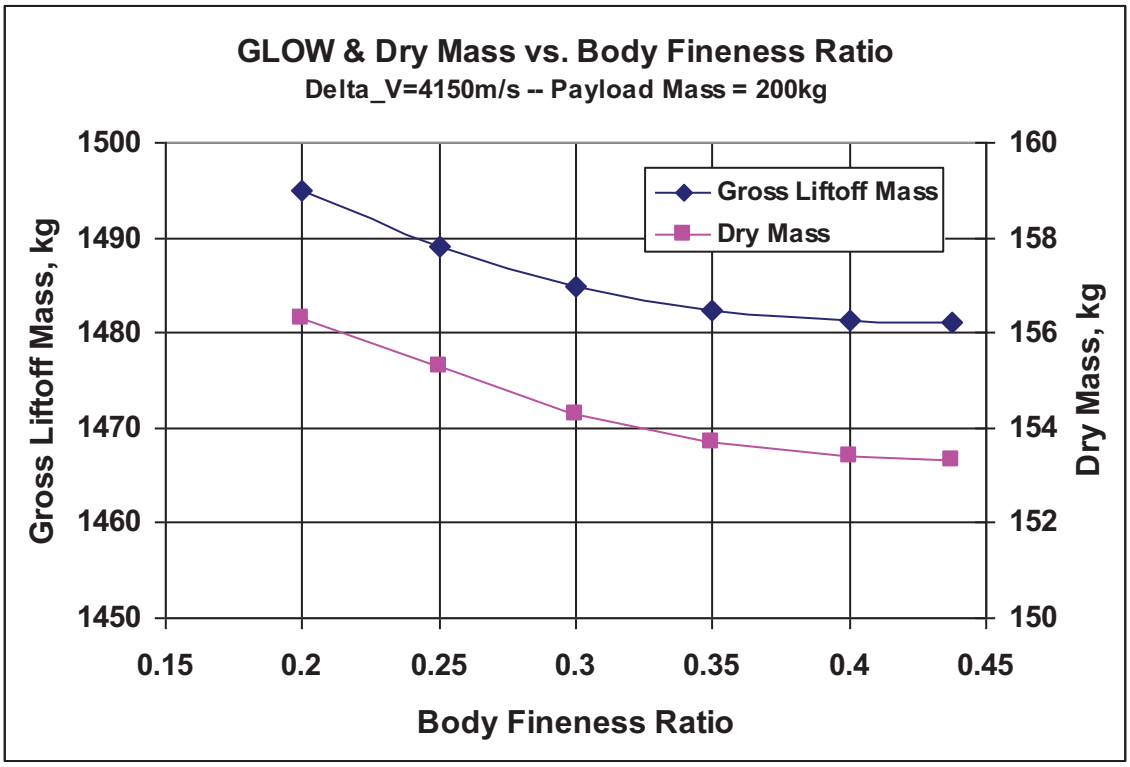


Figure 5.2.3 Overall vehicle length and total wetted area versus body fineness ratio

5.3 Aerodynamics & Aerothermodynamics

Using the surface grids for each of the three parametric shapes, aerodynamic and aerothermodynamic databases were generated for each shape. The aerodynamic database consisted of lift and drag coefficient as a function of Mach number, angle-of-attack and free-stream dynamic pressure. Both engineering-based analysis (References 1 and 2) and Euler CFD codes (Reference 3) were used to compute the aerodynamic coefficients for each shape. The Euler code was used for subsonic, transonic and low supersonic Mach numbers, while the engineering code was run for super and hyper sonic flight conditions. For trade studies that involve forebody shape variations, the aerodynamic coefficients were linearly interpolated with body fineness ratio.

Figure 5.3.1 presents drag coefficient as a function of angle-of-attack and Mach number. For Mach 2.0, both CBAero and Cart3D solutions are shown. The reference area is the cross-sectional area of the body. There is good agreement between the two codes for Mach =2.0, with the drag coefficient higher for the engineering-based model due to viscous drag included. The aerodynamics predicted by CBAero are presented in Figures 5.3.2 through 5.3.4 across the supersonic/hypersonic Mach number range. The effect of the viscous drag at low dynamic pressure on the drag coefficient can be seen in Figure 5.3.2. The aerodynamic database was formatted and provided to the trajectory analysis model to compute lift and drag along the trajectory. As will be discussed below, the aerodynamic impacts on the ascent trajectory are small, due primarily to the low atmospheric density on Mars. Further details of the CFD solutions are presented in Appendix C.

The aero-thermal database was generated using CBAero and consisted of surface pressure, surface shear, convective heat transfer coefficient and recovery enthalpy as a function of Mach number, angle-of-attack and free-stream dynamic pressure. Preliminary estimates of the aero

heating environment were conducted to assess the relative importance of the aero-thermal environment for ascent. The initial analysis indicated that the aero heating environment for the ascent trajectory was rather benign and there would be minimal thermal protection system requirements for the MAV, due again to the low atmospheric density. Sample aero heating results are presented in Appendix C.

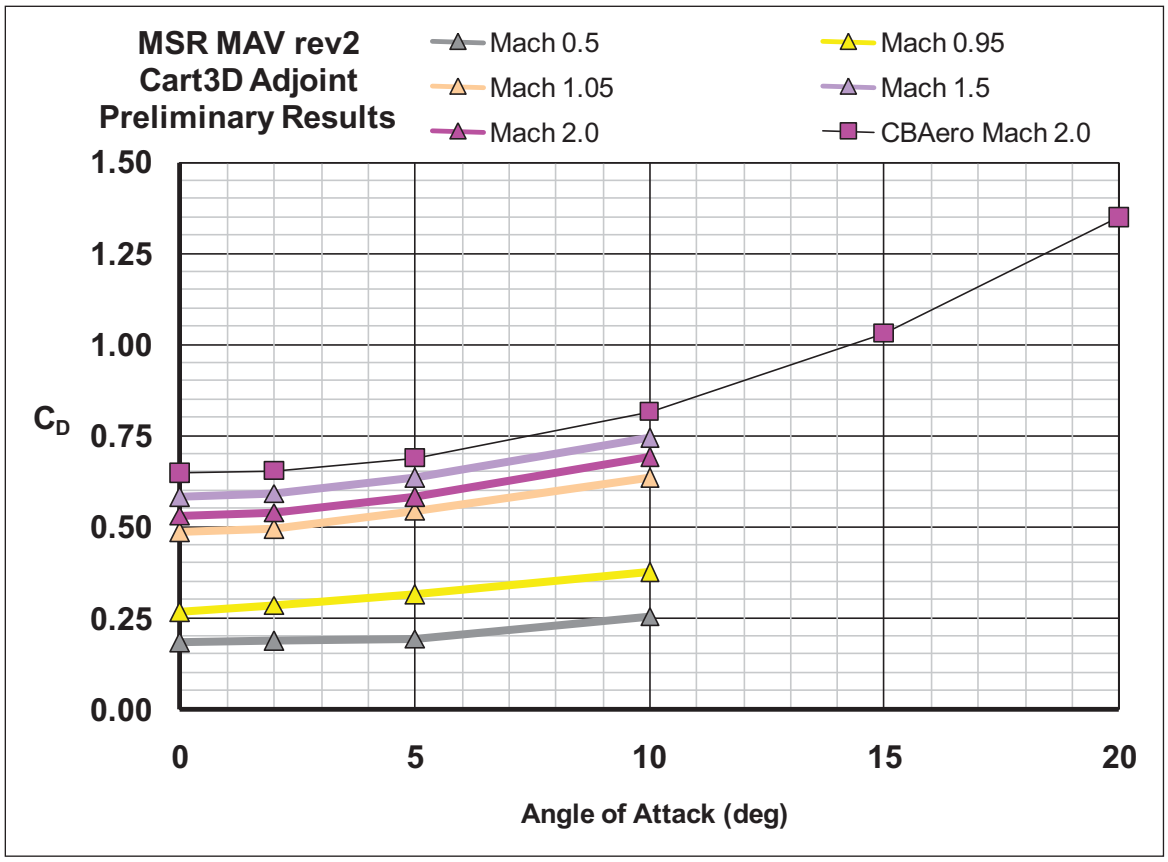


Figure 5.3.1 Drag coefficient versus angle-of-attack and Mach number

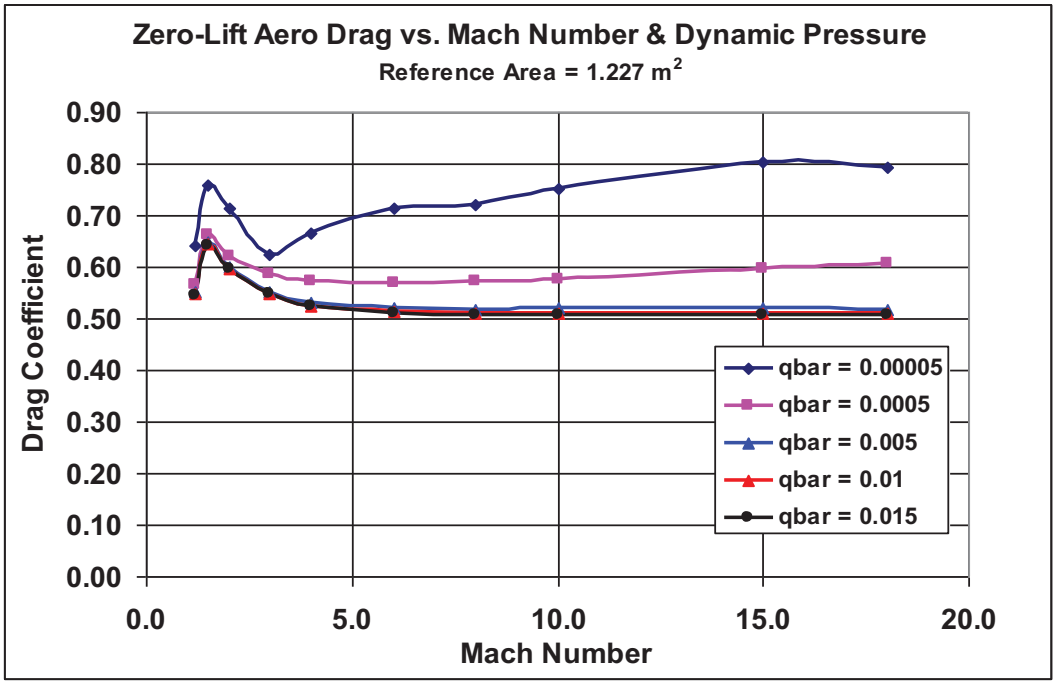


Figure 5.3.2 CBAero predicted zero-lift drag coefficient versus Mach number and free stream dynamic pressure

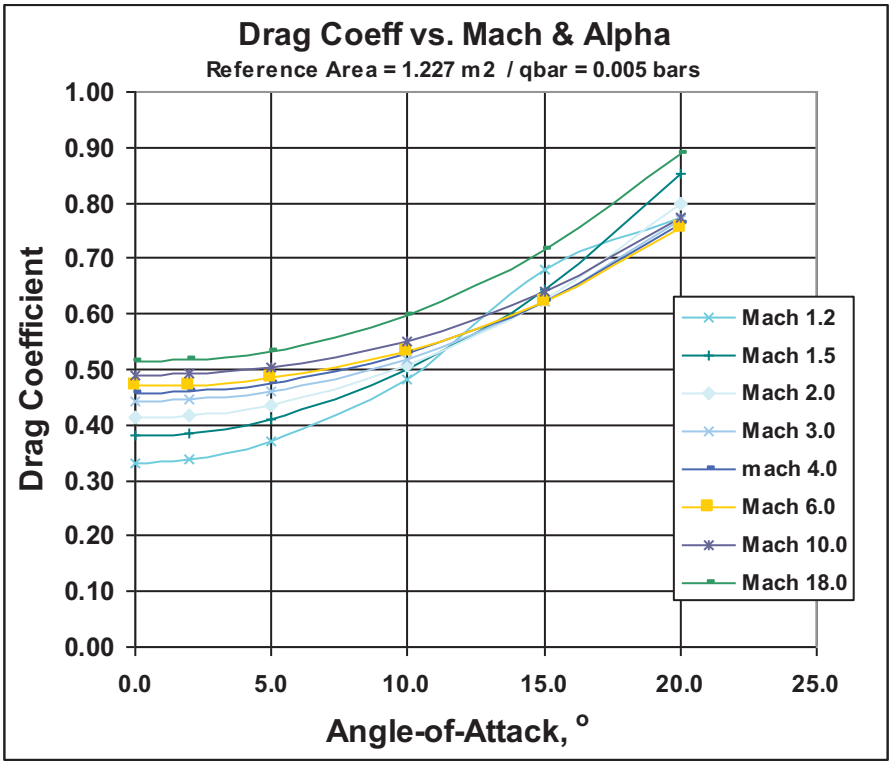


Figure 5.3.3 CBAero predicted drag coefficient versus angle-of-attack and Mach number for dynamic pressure = 0.005 bars

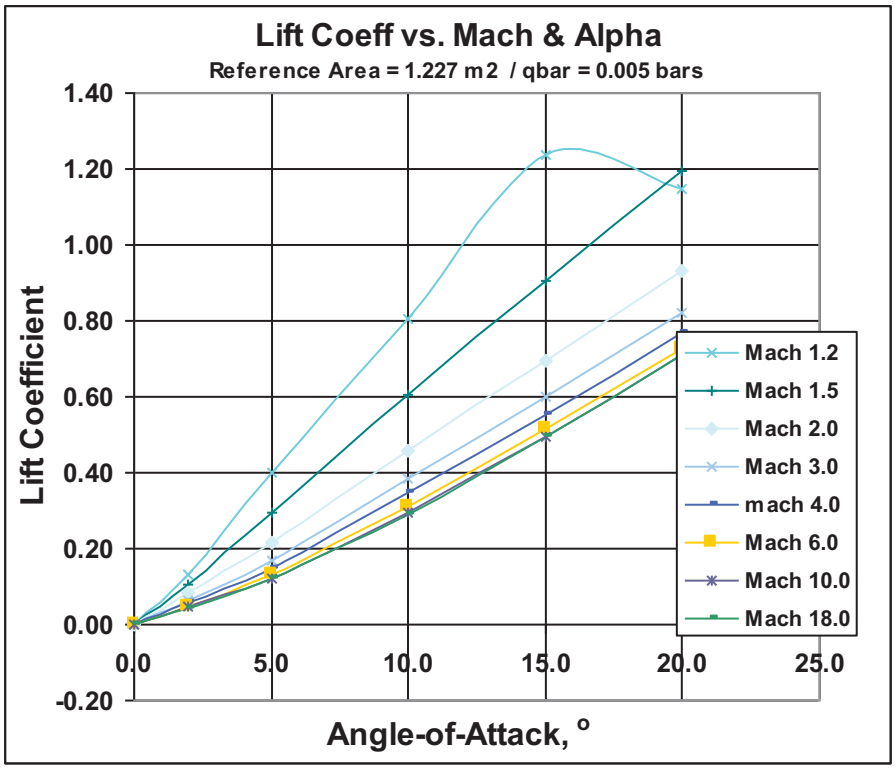


Figure 5.3.4 CBAero predicted lift coefficient versus angle-of-attack and Mach number for dynamic pressure = 0.005 bars

5.4 General Arrangement and Tank Configuration

With potential overall MAV body length constrained by the entry capsule internal volume, a nested tank configuration was selected for the internal arrangement. Similar to a common bulkhead design, the forward tank aft dome is accommodated within a recessed aft tank forward dome but with a purge gap between the two tanks. The inter-tank section is eliminated and the overall vehicle length is reduced. The mated tanks are structural members carrying pressure, axial and bending loads. Thrust loads from the rocket engine are transmitted through a thrust structure and introduced to a load bearing aft compartment, which in turn transmits the thrust loads into the aft tank. The general arrangement is presented in Figure 5.4.1. A forward skirt transitions from the domed tank section into the fore body, which is the fairing for the ERV payload, including a payload adapter. The nested tank internal configuration is shown in Figure 5.4.2. The oxidizer tank is forward, resulting in forward axial center-of-gravity, reducing engine gimbal requirement for trim.

High temperature polymer matrix composite thermo-plastic (PEEK) was chosen for the material for the aero-shell, tank (with a liner), aft compartment and thrust structure. The aft compartment and tanks were sized based on loads using mass estimating relationships (see below) and the forward aero-shell assumed to be minimum gauge skin-stringer stiffened structure, consisting of 5 skin plies + stiffeners, with an areal mass of 1.04 kg/m^2.

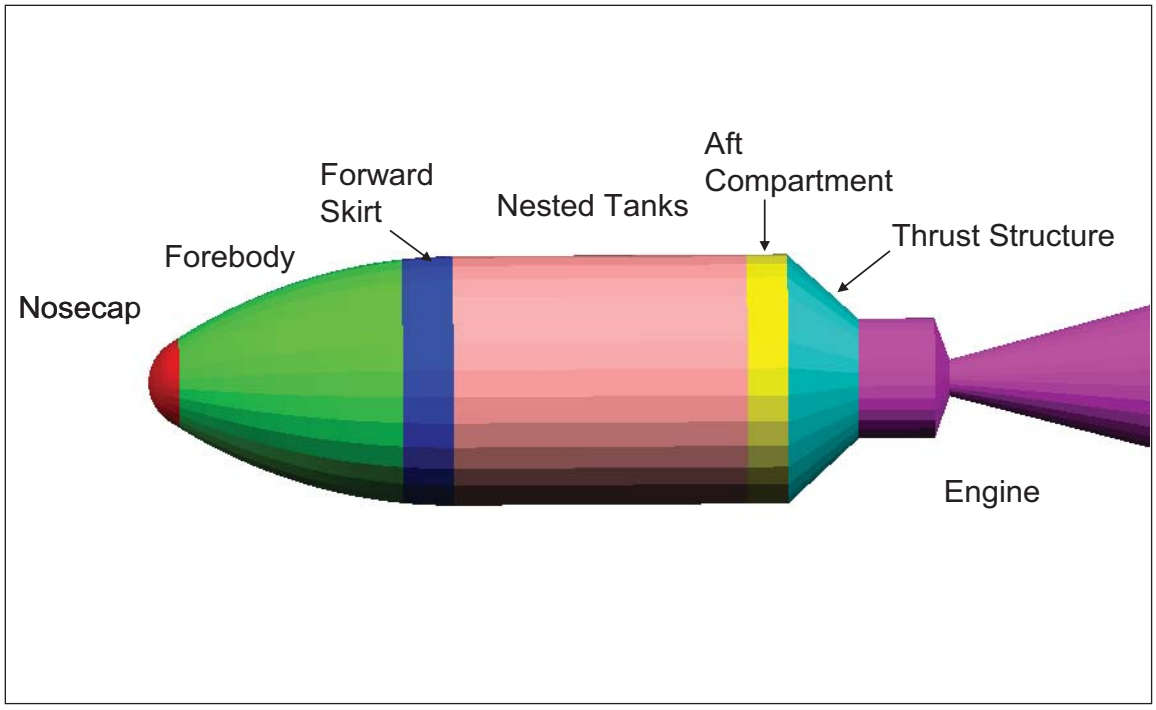


Figure 5.4.1 MAV general arrangement

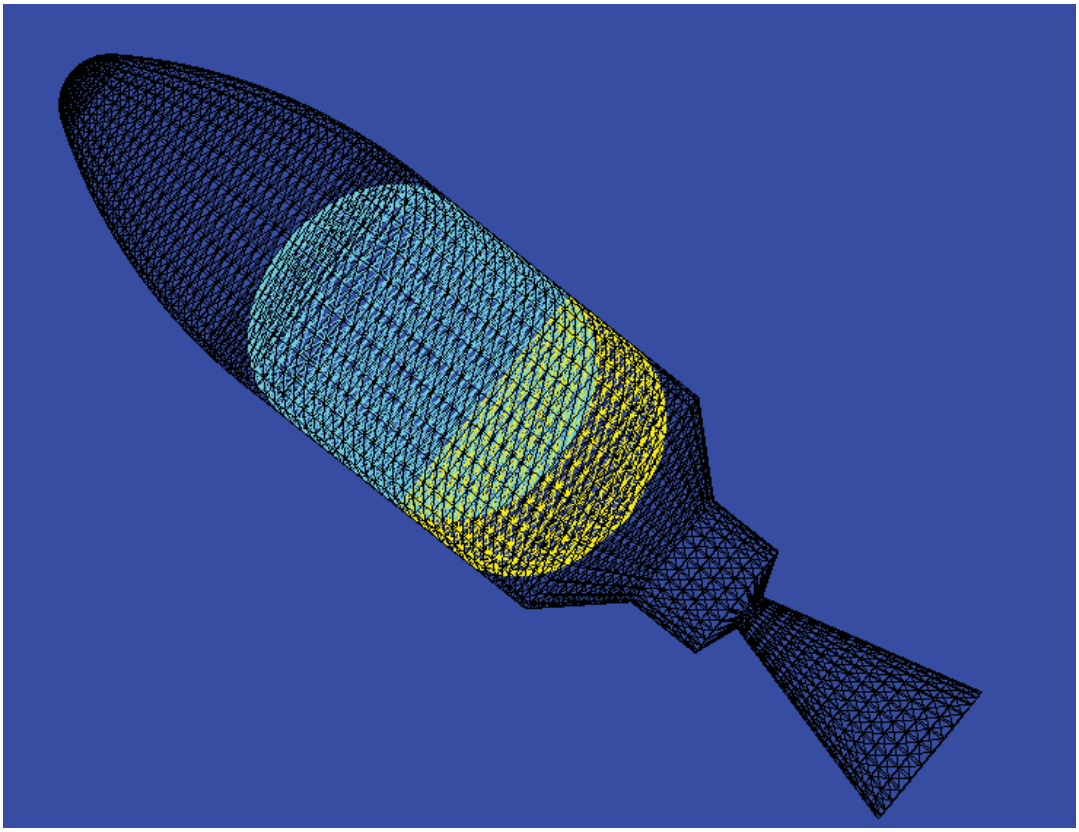


Figure 5.4.2 MAV internal arrangement

5.5 Mass Estimating Relationships

The mass of the vehicle subsystems was computed using mass estimating relationships (MER's), taken from various sources (References 4, 5, 6, 5 and 8). Generally, the MER's are based on historical data correlated to pertinent design parameters for existing launch vehicles. The scale of the MAV concept was found to be typically at the low end of the correlated data, or completely outside the data range, resulting in some extrapolation for certain subsystem elements. An example (taken from Reference 5) is presented in Figure 5.5.1 for the unit areal mass of the inter-tank and aft compartment, based on unit axial load, body diameter and material property. The range of the axial loads for the MAV configuration is indicated in the lower left hand corner. Knowing the inertial load at the maximum 5.0 Earth's axial acceleration and apply a factor-of-safety = 1.4, the areal weight of the aft compartment is computed from Figure 5.5.1 and multiplied by the wetted area of the aft compartment to obtain its mass.

In addition to structural and tank mass, MER's were assembled from the above references for other subsystems, including induced environments, auxiliary systems (separation systems), main propulsion (main engines, feed/pressurization and controls), prime power systems (batteries and pneumatic systems for engine control), power conversion and distribution and data handling/communication/control (DHCC). Figure 5.5.2 presents the mass scaling model for the main propulsion engine, with engine thrust-to-weight ratio value plotted as a function of engine thrust. Generally the engine thrust-to-weight goes down in decreasing thrust level, reflecting the impact of minimum gauge on smaller engines. The engines shown in Figure 5.5.2 are generally pressure-feed OMS/RCS engines. The reference XLF-132 pump feed engine is also plotted. The mass of the scaled pump-feed engine was then computed using the required vacuum thrust and the shifted trend line of engine thrust-to-weight versus engine thrust (shifted to pass through the XLR-132 data point, but having the same slope).

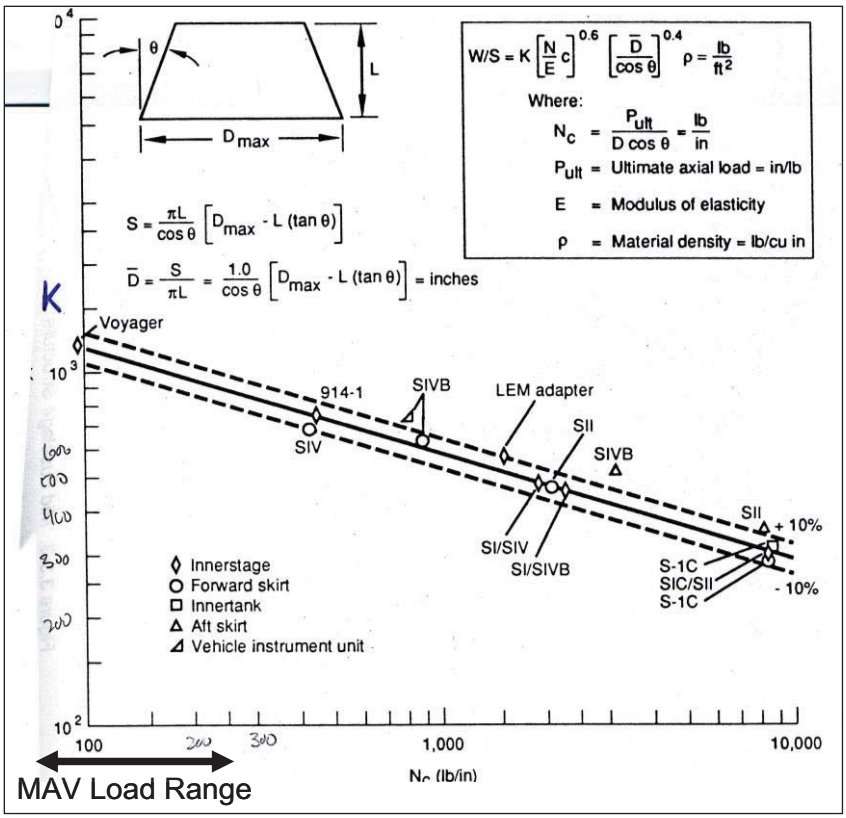


Figure 5.5.1 Inter-tank and aft compartment structure mass estimate model (taken from Reference 5)

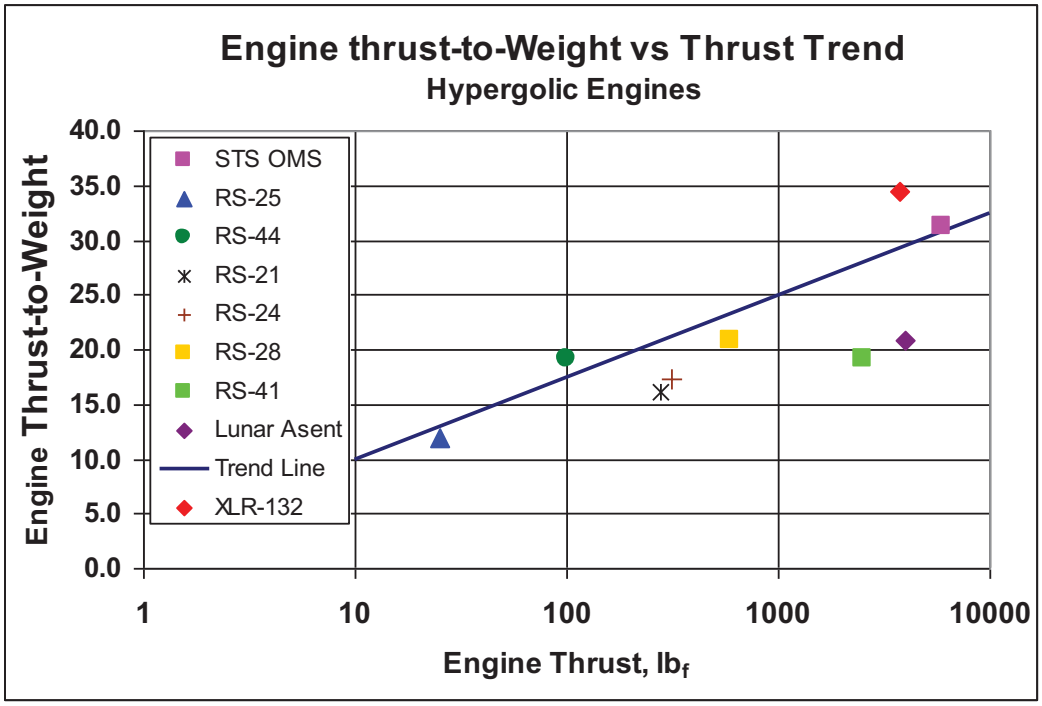


Figure 5.5.2 Rocket engine weight-to-thrust ratio versus engine thrust

6.0 Ascent Trajectory

The ascent trajectory for the MAV was simulated using POSTII (Reference 9). Aerodynamic tables of lift and drag coefficient were provided as a function of Mach number, dynamic pressure and angle-of-attack (Section 5.3). Rocket engine performance model consisted of engine vacuum specific impulse and nozzle exit area. The 3 DOF trajectory was optimized for maximum burn-out mass, with control parameters of angle-of-attack, bank angle and liftoff vehicle thrust-to-weight. The Mars GRAM atmospheric model 2001 was used. The launch point was 0m MOLA altitude, 0º Latitude and 0º Longitude, heading due East. Constraints on maximum dynamic pressure, maximum q-alpha and final altitude were imposed. Three orbital ascent trajectories were computed: 100 X 100 km, 100 X 500 km, and 500 X 500 km and C_3=0 at 500 km, the total ΔV calculated for each.

Figures 6.1 through 6.5 present the optimized ascent trajectory history for the 100 X 500 km orbital case. Figure 6.1 and 6.2 present altitude as a function of Mach number and time, respectively. Ascent time is approximately 265 seconds. The dynamic pressure time history is shown in Figure 6.3, with a maximum value of 250 Pa, which occurs at approximately Mach = 1.6. The total acceleration as a function of time is presented in Figure 6.4, with a burn out maximum 5.3 Mars g's. Figure 6.5 presents the optimal control for the MAV ascent trajectory, with angle-of-attack and bank angle shown as a function of time. The vehicle is banked to a "heads-down" attitude, initiated at roughly 30 seconds after liftoff.

Table 1 summarizes the total ΔV required for the three orbital and two escape cases. Also noted is the final-to-initial mass ratio required for each, assuming an engine specific impulse of 343 seconds. Finally, the relative velocity loss breakdown for the 100 X 500 km orbital and the escape trajectories are presented in Figures 6.6 and 6.7. For both cases, the drag, thrust vectoring and atmospheric losses are all small.

Table 1 Ascent Velocities and mass fractions

Orbit (km)	Velocity (m/s)	ΔV (m/s)	m/m_o
(100,100)	3503	4027.9	0.3019
(100, 500)	(3597,3227)	4115.5	0.2942
(500, 500)	3318.1	4206.7	0.2862
C3-0 @100km	4951.2	5476.1	0.1962
C3=0 @500km	4690	5578	0.1904

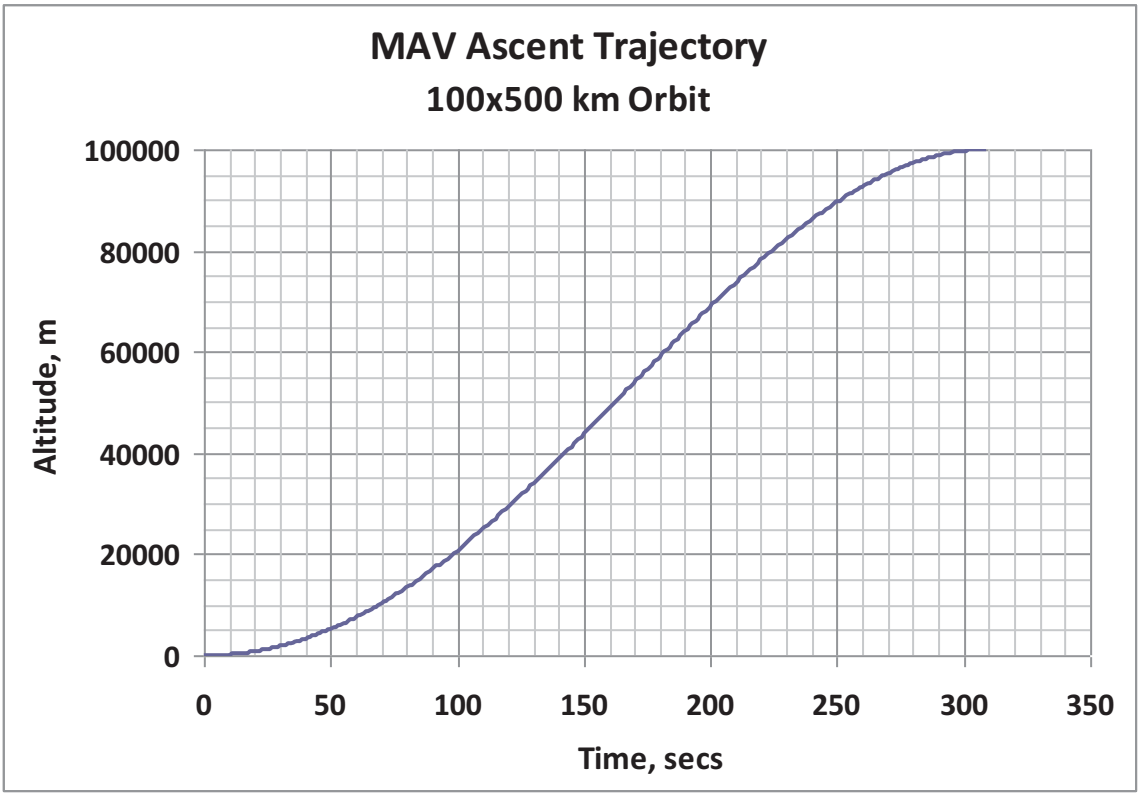


Figure 6.1 MAV ascent trajectory: Altitude versus time

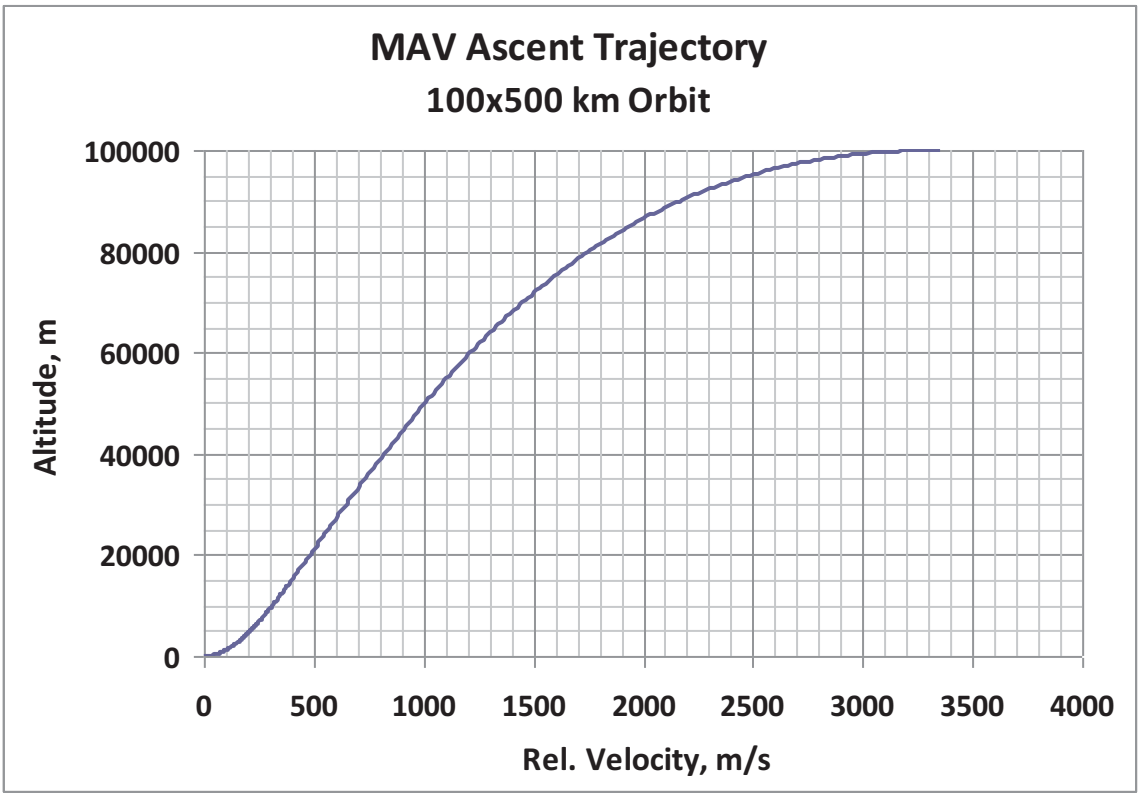


Figure 6.2 MAV ascent trajectory: Altitude versus relative velocity

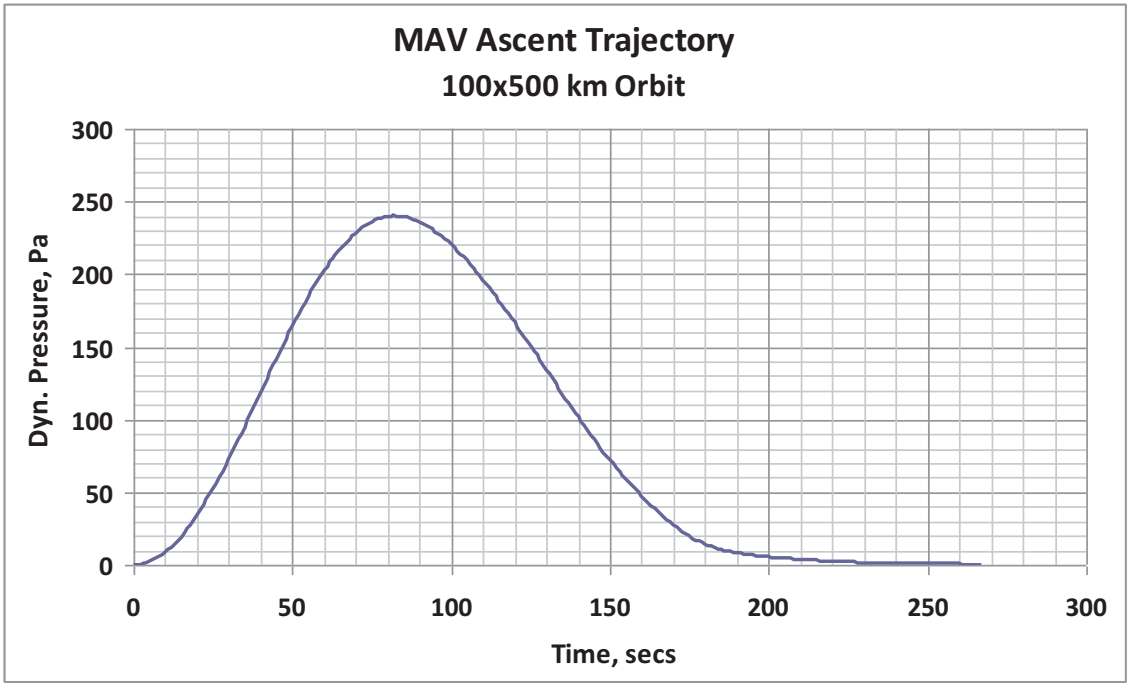


Figure 6.3 MAV ascent trajectory: Dynamic pressure versus time

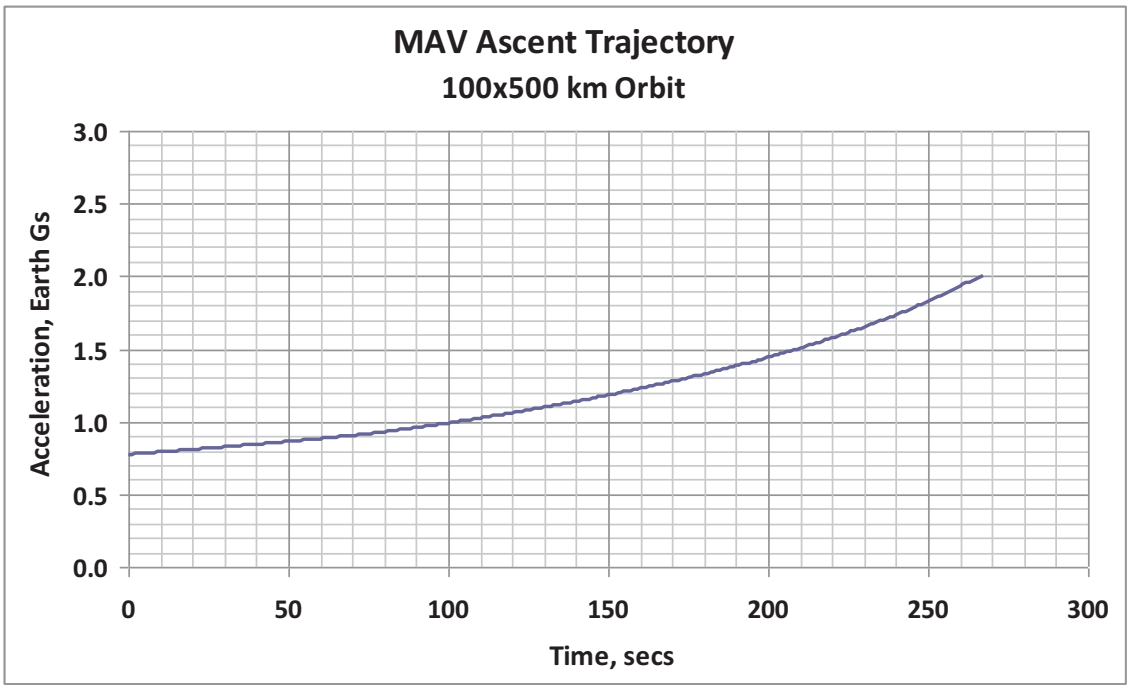


Figure 6.4 MAV ascent trajectory: Acceleration versus time

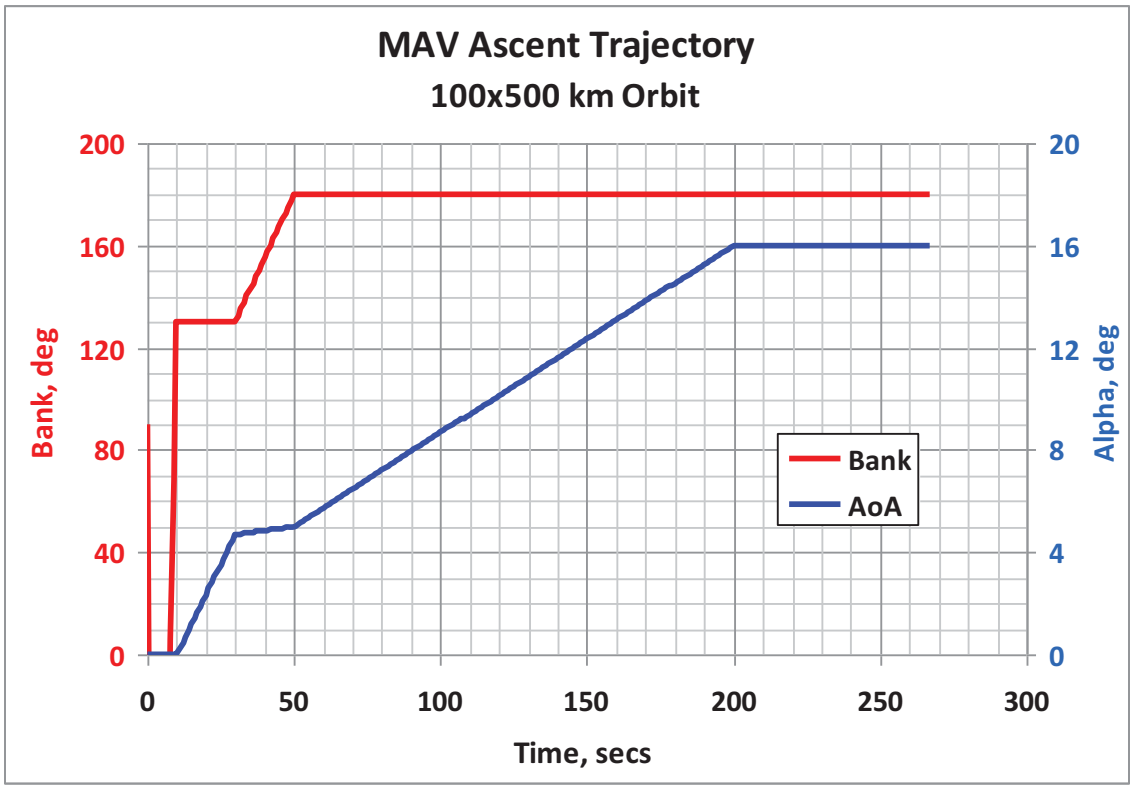


Figure 6.5 MAV ascent trajectory: Dynamic pressure versus relative velocity

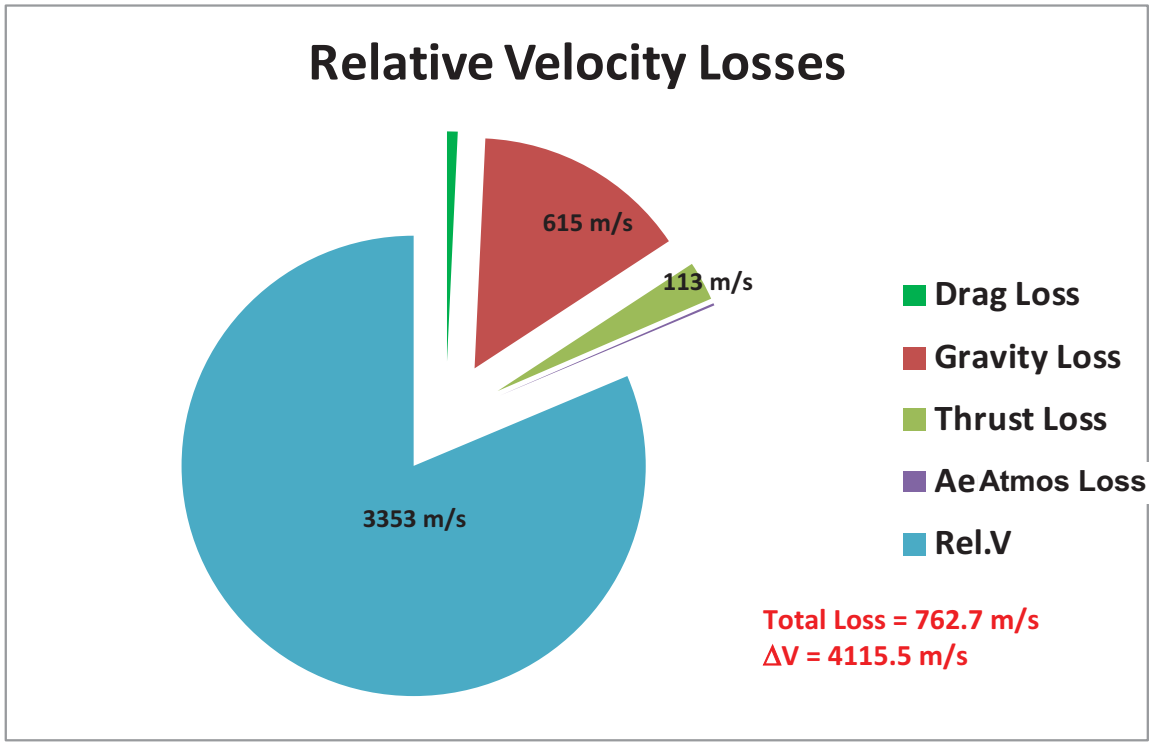


Figure 6.6 Orbital relative velocity loss breakdown

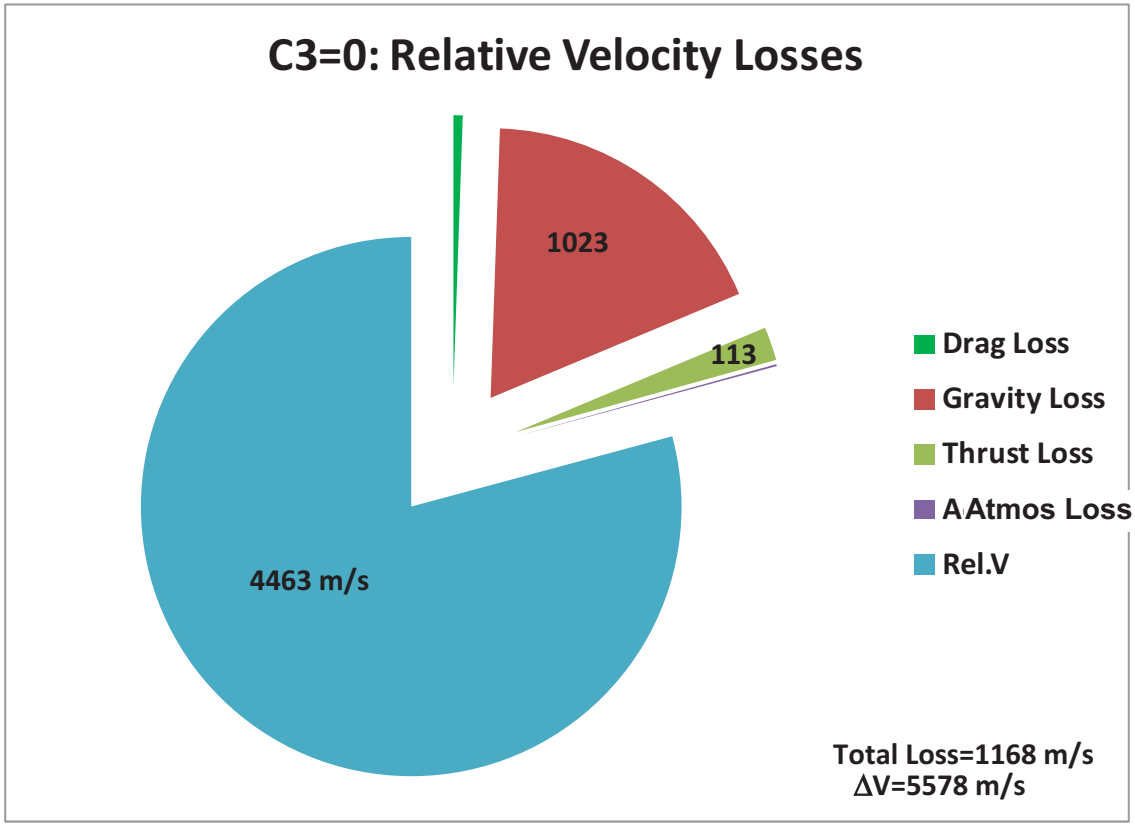


Figure 6.7 Escape relative velocity loss breakdown

7.0 Baseline Configurations

Two MAV architectures were initially examined, one to launch a prescribed payload to orbital flight conditions for Mars orbital rendezvous (inert payload) or phasing orbit for Earth return by an ERV, and a second to escape velocity conditions for Earth orbital rendezvous. The payload mass was initially treated parametrically to capture the impact of the payload mass and volume on the MAV design requirements. These baseline configurations were then used as the reference point for the trade studies.

7.1 Vehicle Closure

Initial vehicle sizing was conducted using the assumptions stated above in Section 4.0 for the baseline configuration and engine, as described in Section 5.1 and 5.2. Total ΔV's for orbital and escape missions presented in Section 6.0 where used for determining propellant fraction required. A vehicle synthesis code was developed using the subsystem MER's and a first cut geometry/packing model to compute propellant fraction available and required volume for all subsystems. For both the orbital and escape architectures, a range of payload masses were examined and the vehicle closed by matching propellant fraction required to propellant fraction available using the vehicle synthesis model.

7.2 Orbital Architecture

The Mar's orbital architecture MAV places either an inert capsule (assumed mass of 20 kg for orbital rendezvous) or a chemical powered ERV (mass ranging from say 80 to 200 kg) into low Mars orbit, with the required total ΔV = 4150 m/sec. For either payload, an assumed payload density of 400 kg/m^3 was used to compute the payload volume. The MAV was then sized to provide sufficient payload, propellant tankage and subsystem mass and volume to perform the mission.

Figure 7.2.1 presents the vehicle closure plot, showing propellant fraction required and propellant fraction available as a function of gross liftoff mass for a fixed payload requirement. The propellant fraction required is a function only of the required total ΔV and the engine specific impulse. Due to the low density of the Martian atmosphere, hence low aerodynamic drag on ascent, the engine specific impulse and the vehicle specific impulse are almost the same and as a result the propellant fraction required becomes independent of the vehicle mass (size). The intersection of the propellant fraction required and propellant fraction available represents a closed vehicle design. As the payload requirement is increased the closure GLOM also increases, but so does the payload mass fraction, ranging from roughly 6% at 20kg payload mass to about 13% at 200 kg.

An important characteristic of the vehicle design is the slope of the propellant fraction available at the intersection point. As mission requirements or engine performance characteristics change, the propellant fraction required may shift up or down. Subsystem technology or performance may also vary, resulting in a shift of the propellant fraction available curve. If the slope of the propellant fraction available curve at the intersection point is shallow, small changes in either the propellant fraction available or propellant fraction required will result in relatively large shifts in the intersection point, hence relatively large changes in the closure gross mass. The steeper the propellant fraction available curve at the intersection point, the less sensitive the vehicle closure mass to shifts in either propellant fraction curve. As seen in Figure 7.2.1, the slope of the propellant fraction available curve tends to decrease with increasing GLOM. Hence, at higher payload mass requirements, both the required vehicle launch mass increases and the design becomes more sensitive to mission requirements or technology performance.

Another measure of design robustness is often presented in terms of a “growth factor”: the amount the vehicle will grow for every additional kilogram of mass required to be carried to orbit. Table 2 summarizes the salient characteristics, including some subsystems masses, dry mass and gross liftoff mass, dimensions and growth factor of the orbital architecture for the various payload requirements. For the orbital architecture concepts, every kilogram added is roughly 6 more kilograms of gross liftoff mass. For the baseline 200 kg payload design, Figure 7.2.2 presents overall vehicle dimensions (not to scale).

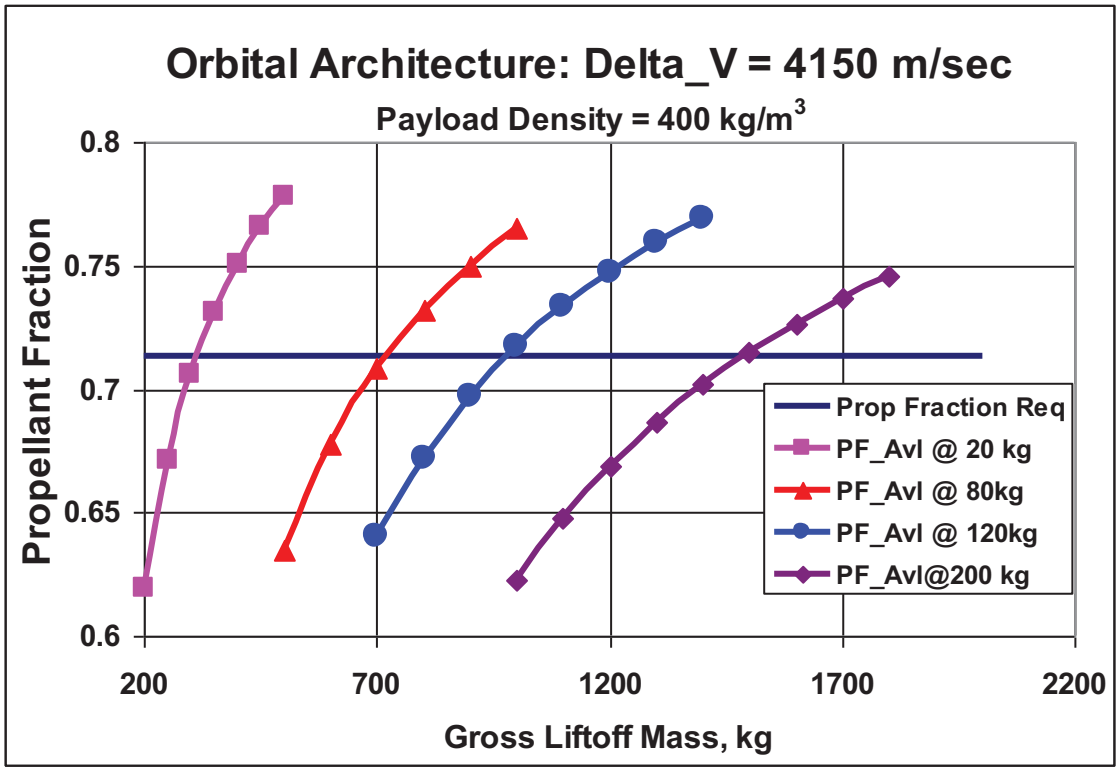


Figure 7.2.1 Orbital architecture closure point versus GLOM and payload mass

Table 2. Orbital architecture characteristics

Payload Mass	20 kg	80 kg	120 kg	200 kg
Tanks, kg	5.7	11.8	15.5	22.4
Total Structure, kg	9.4	21.3	28.6	42.5
Main Engine, kg	19.4	27.4	31.8	39.9
Main Propulsion, kg	24.1	33.9	39.4	49.3
Dry Mass, kg	54.0	90.6	112.5	154.1
Dry Mass fraction, %	17.3	12.6	11.5	10.4
GLOW, kg	312.5	717.4	976.7	1484.
Length, m	2.19	3.02	3.38	3.95
Diameter, m	0.52	0.71	0.79	0.91
Growth Factor	6.8	6.7	6.5	6.3

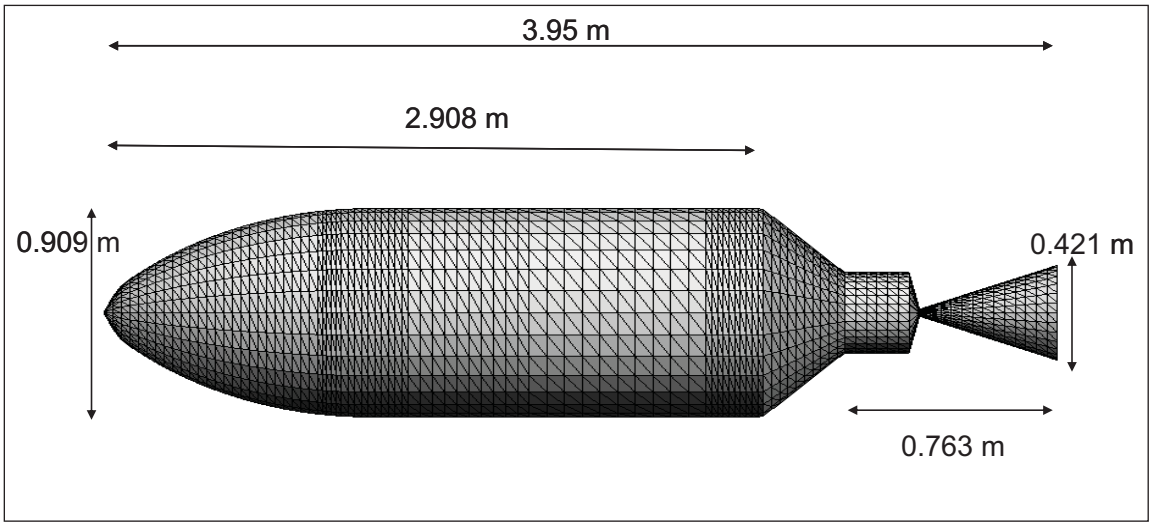


Figure 7.2.2 Orbital Architecture, 200 kg payload MAV dimensions

7.3 C_3=0 Architecture

The Mars' escape architecture MAV accelerates an ERV (mass ranging from say 20 to 200 kg) to $C_3 = 0$, with the required total $\Delta V = 5500$ m/sec. For this mission, it was assumed that the ERV would be solar-electric powered (SEP), rather than chemical powered used for the orbital architecture concept. An assumed payload density of 240 kg/m^3 was used to compute the payload volume, reflecting the less compact SEP configuration.

Figure 7.3.1 presents the vehicle closure plot, showing propellant fraction required and propellant fraction available as a function of gross liftoff mass for a fixed payload requirement. Again, the intersection of the propellant fraction required and propellant fraction available represents a closed vehicle design. As the payload requirement is increased, the closure GLOM also increases, but so does the payload mass fraction, ranging from roughly 2.6% at 20kg payload mass to about 6.2% at 200 kg. Table 3 summarizes the salient characteristics, including some subsystems masses, dry mass and gross liftoff mass, dimensions and growth factor of the orbital architecture for the various payload requirements. For the escape architecture concepts, the growth factor in on the order of 13 kg added for every additional 1 kg, roughly twice that of the orbital architecture concepts. For the baseline 120 kg payload design, Figure 7.3.2 presents overall vehicle dimensions.

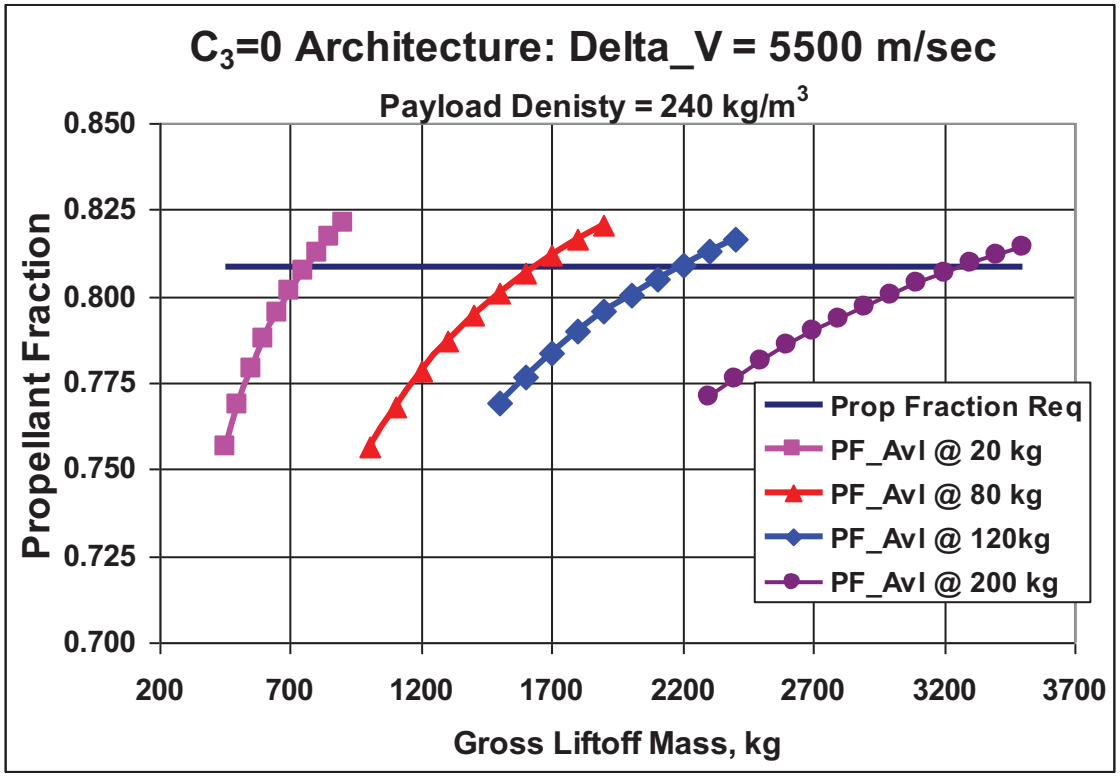


Figure 7.3.1 C_3=0 architecture closure mass versus GLOM and payload mass

Table 3. Escape architecture characteristics

Payload Mass	20 kg	80 kg	120 kg	200 kg
Tanks, kg	13.8	27.1	35.1	49.7
Total Structure, kg	19.6	40.7	54.1	79.1
Main Engine, kg	28.1	42.1	50.4	65.4
Main Propulsion, kg	34.9	52.2	62.4	80.9
Dry Mass, kg	83.7	144.1	181.6	251.4
Dry Mass fraction, %	11.0	8.8	8.3	7.7
GLOW, kg	758	1628	2187	3247
Length, m	2.99	4.03	4.52	5.26
Diameter, m	0.70	0.92	1.03	1.19
Growth Factor	14.4	13.8	13.5	13.2

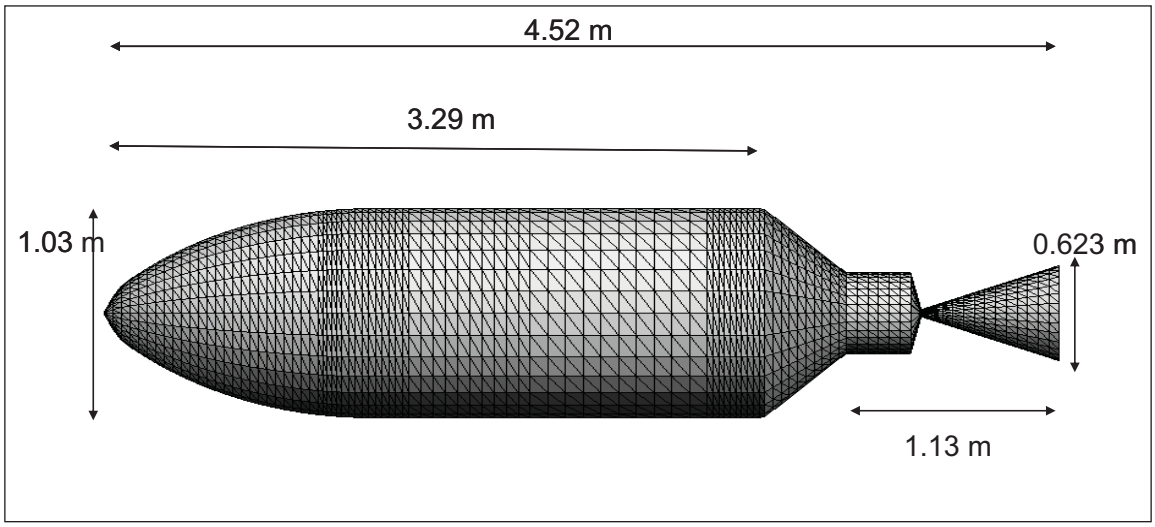


Figure 7.3.2 C3=0, 120 kg payload MAV dimensions

8.0 Trade Studies

With the baseline MAV designs established, trade studies were conducted to look at alternate design approaches and technologies. The goal was to explore the design space and identify the most promising configurations and candidate technologies and determine design sensitivities. The trade studies were typically conducted for one payload class, rather than over the range of assumed payload masses.

8.1 Number of Engines

The baseline configuration consisted of a single gimbaled engine with pneumatic thrust vectoring control. An alternate configuration is to use multiple expansion nozzles with a common power head, and variable engine thrust to achieve pitch and yaw control. Roll control would continue to use gas-generator exhaust flow. A 15% penalty in power head mass was assumed for multiple engine feeds, and the weight of the thrust structure increases with the number of engines. The trade study was conducted for the orbital architecture.

Table 4 presents a comparison between the baseline single engine and a 3 and 4 engine nozzle configuration for a fixed liftoff mass of 1500 kg. The total thrust for all three configurations is the same. The multiple engine design approach results in overall engine length being significantly shorter, but still allows engine integration into the base region of the vehicle without requiring any aft skirt fairing. Thrust structure and aft compartment mass increase with number of engines, while engine heat shield and base close-out TPS decrease due to reduced wetted areas. Engine total mass and propellant feed system mass show small variations. The biggest mass savings for the multiple engine configuration is in the elimination of the engine gimbal control and associated pneumatic prime power elements. For the fixed launch mass, the 3 and 4 engine configurations save roughly 4% in dry mass, with the 3 engine configuration having a slight edge in propellant fraction available. From a closed mass perspective, the multiple engine configuration saves approximately 4% in dry mass and roughly 2% in liftoff mass. The last two rows of Table 4 present the closed vehicle dry mass and gross liftoff mass.

Table 4 Number of Engine comparison

No. Engines	1	3	4
Engine Thrust, N	13950	4650	3488
Engine Diameter/Length, m	0.423 / 0.767	0.245 / 0.443	0.212 / 0.384
Engine Thrust-to-Weight	35.39	34.38	34.34
Thrust Structure length, m	0.276	0.187	0.191
Aft Compartment Length, m	0.120	0.205	0.202
Thrust Structure wetted area, m^2	0.778	0.610	0.617
Aft Compartment wetted area, m^2	0.344	0.593	0.583
Thrust Structure mass, kg	4.67	6.86	7.56
Aft Compartment mass, kg	1.26	2.17	2.13
Engine Heat Shield mass, kg	0.70	0.23	0.17
Base Close-out TPS mass, kg	1.66	0.55	0.42
Main Engine Mass, kg	40.16	41.38	41.83
Propellant Feed System mass, kg	2.87	2.74	2.72
Engine Gimbal/Control mass, kg	5.83	0.	0.
Prime Power, Pneumatics mass, kg	2.35	0.	0.
Dry Mass, kg	154.9	148.2	148.7
Propellant Fraction Available, %	71.5	71.93	71.88
Closed Dry Mass, kg	154.1	145.8	146.5
Closed Gross Lift-off Mass. kg	1484	1450	1455

8.2 Pressure-Feed Propulsion System

The baseline engine concept is a gas-generator cycle with turbo-pump propellant feed. This design approach results in significant tank mass savings due to the lower required tank pressure. For the small payload mass (20kg inert capsule), the sized MAV vehicle is in 200 to 300 kg class range, resulting in engine thrust levels on the order of ~2000 N. This represents a scaling of the engine down to approximately 15% of baseline XLR-132 engine thrust level. Scaling a turbo-pump feed engine by a factor of 7 may incur significant performance penalties, which were not modeled in the current study. As a result, a pressure-feed propulsion system was studied and two vehicle classes were evaluated: 1) 20kg payload orbital vehicle, and 2) 200 kg payload orbital vehicle. For each design the effect of chamber pressure and nozzle expansion ratio were assessed. Both cases utilize hypergolic propellants.

Appendix A presents the impact of chamber pressure and nozzle expansion ratio on engine specific impulse, thrust per unit exit area and engine mass. For the 20 kg payload mass, Figure 8.2.1 presents the propellant mass fraction required as a function of the chamber pressure. There is a modest increase in the engine specific impulse with higher chamber pressure, hence a modest reduction of the propellant fraction required. For the closed vehicle, the overall vehicle length decreases with increasing chamber pressure ratio (see Figure 8.2.2), reflected directly to the increase in thrust per unit area at higher chamber pressure, hence a smaller, shorter engine. The trend flattens out at higher chamber pressures as a result of body length increases at the higher pressures. Figure 8.2.3 shows tank, pressurization system and engine mass as a function of thrust chamber pressure. As the pressure increases, the tank mass and pressurization system mass increase, while the engine mass decreases due to a physically smaller engine at higher chamber pressure, even though the unit area mass of the engine nozzle increases with chamber pressure. Finally, Figure 8.2.4 presents closed dry mass and gross liftoff mass as function of chamber pressure. The offsetting effects of tank and pressurization system mass versus engine mass results in a minimum of both dry and gross mass, occurring near a chamber pressure around 1.03MPa (150 psi).

Table 5 summarizes the comparison of the pump-feed versus the pressure feed engine system. The tank mass and pressurization system are significantly higher for the pressure feed system compared to the pump feed design, with the main engine mass ~15% lighter. The resulting dry mass for the pressure feed system is 21% higher, with the propellant fraction only slightly higher. The closed gross liftoff mass is on the order of 26% heavier and 20% longer. For the 20 kg payload class, both concepts are comfortably below the maximum landed payload mass limit, and the pressure feed concept would be viable if the engine scaling issues associated with the pump feed system become limiting.

The pressure feed trade study was repeated for a 200 kg payload mass requirement. At this scale, the pressure feed system is almost twice the gross liftoff mass as the equivalent pump feed system. As the propellant tanks become large, the tank mass increases rapidly and the dry mass and gross mass grow significantly. Figure 8.2.6 shows closed dry mass and gross liftoff mass as a function of chamber pressure. Dry mass is fairly insensitive to chamber (i.e. propellant tank pressure), again trading tank and pressurization system mass versus engine mass, and a minimum in gross mass occurs somewhat below 1.38 MPa (200 psi). Figure 8.2.7 presents overall vehicle length as a function of engine chamber pressure, with significantly longer vehicles at the lower engine pressure. Table 6 summarizes the comparison of the two concepts for the 200 kg payload mass. The pressure feed systems becomes noncompetitive with the pump feed system and violates the maximum allowable landed mass and vehicle overall length by roughly 30% to 40%.

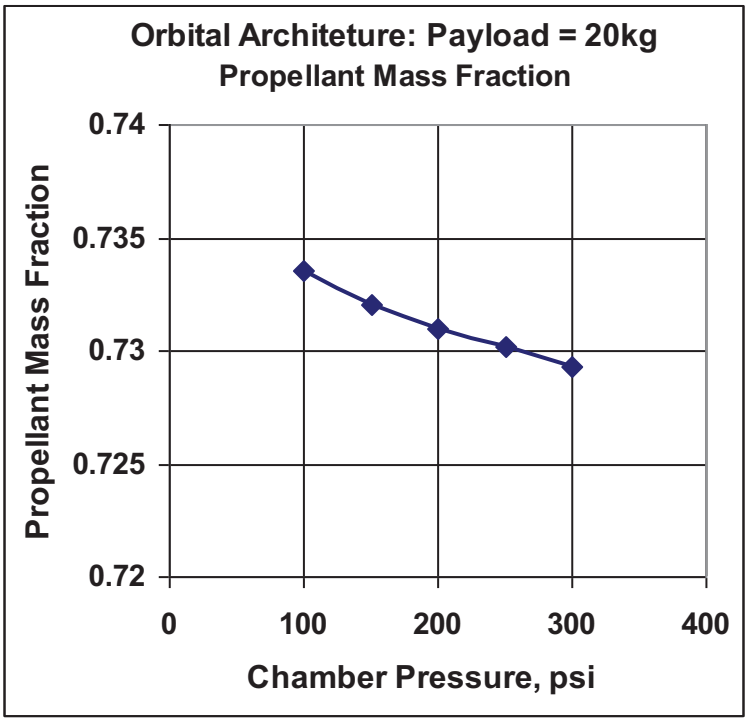


Figure 8.2.1 Propellant fraction required versus chamber pressure

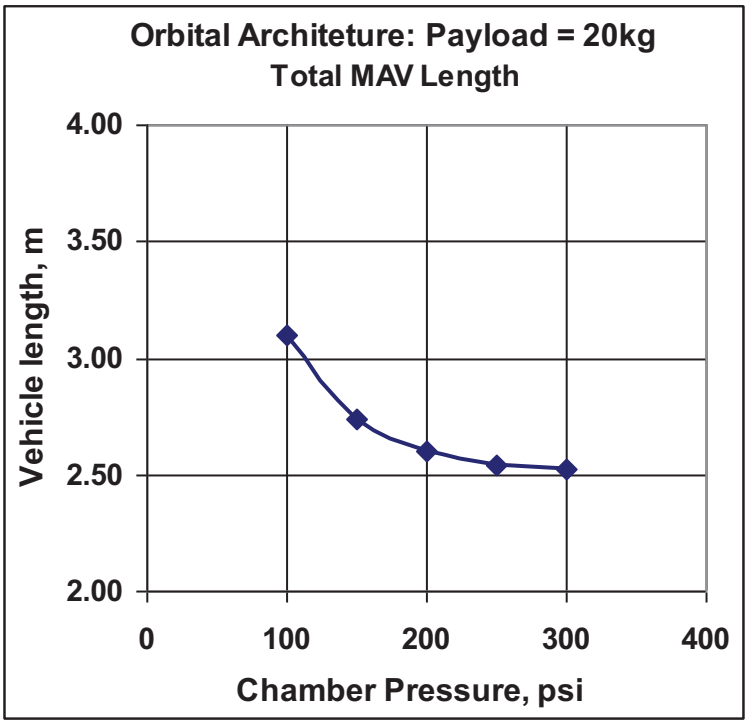


Figure 8.2.2 Overall vehicle length versus chamber pressure

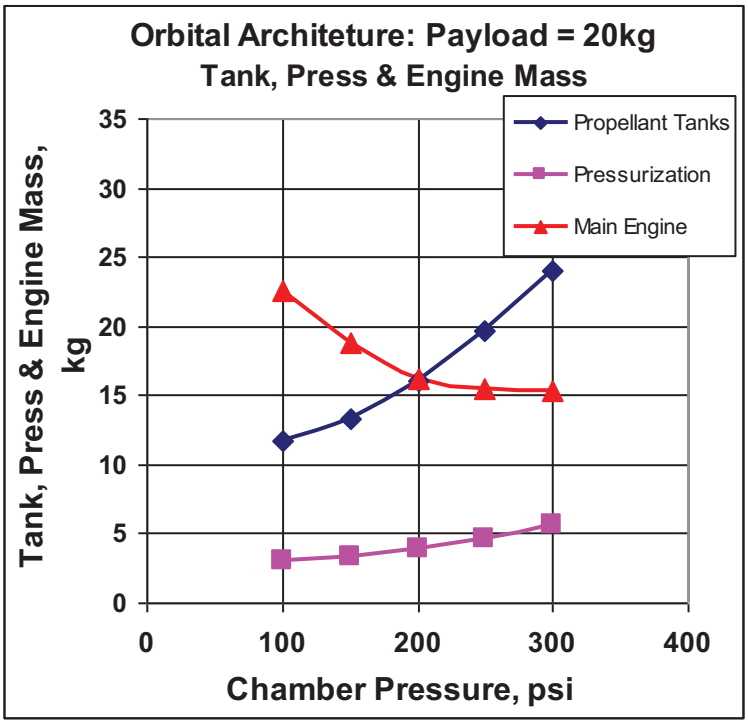


Figure 8.2.3 Tank, pressurization and engine mass versus chamber pressure

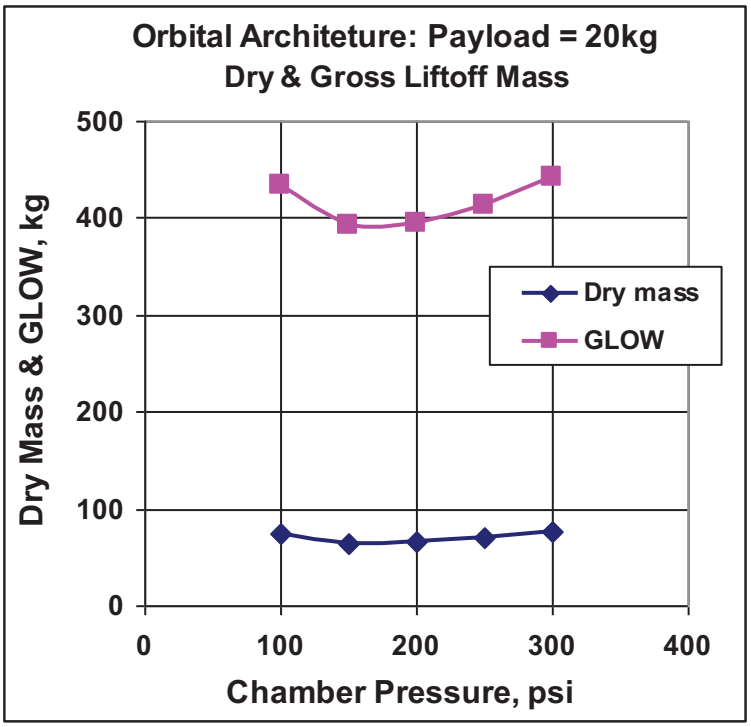


Figure 8.2.4 GLOW and dry mass versus chamber pressure

Table 5. 20kg payload pump feed versus pressure feed system comparison

	Pump Feed	Pressure Feed
Tank Pressure	**0.034 MPa (5.0 psi)**	**1.30 MPa (188 psi)**
Tanks	**5.70 kg (13.7% Dry)**	**16.04 kg (31.8% Dry)**
Structure	**9.23 kg (22.2% Dry)**	**21.26 kg (42.2% Dry)**
Main Engine	**19.2 kg (46.8% Dry)**	**16.27 kg (32.3% Dry)**
Pressurization	**0.92 kg (2.2% Dry)**	**3.91 kg (7.8% Dry)**
Main Propulsion	**24.1 kg (46.8% Dry)**	**20.38 (40.4% Dry)**
Dry Mass	**54.0 kg (17.3% GLOW)**	**65.5 kg (16.6% GLOW)**
Propellant Fraction	**71.3%**	**73.1%**
GLOW	**312.5 kg**	**394.1 kg**
Length	**2.19 m**	**2.60 m**
Diameter	**0.520 m**	**0.566 m**

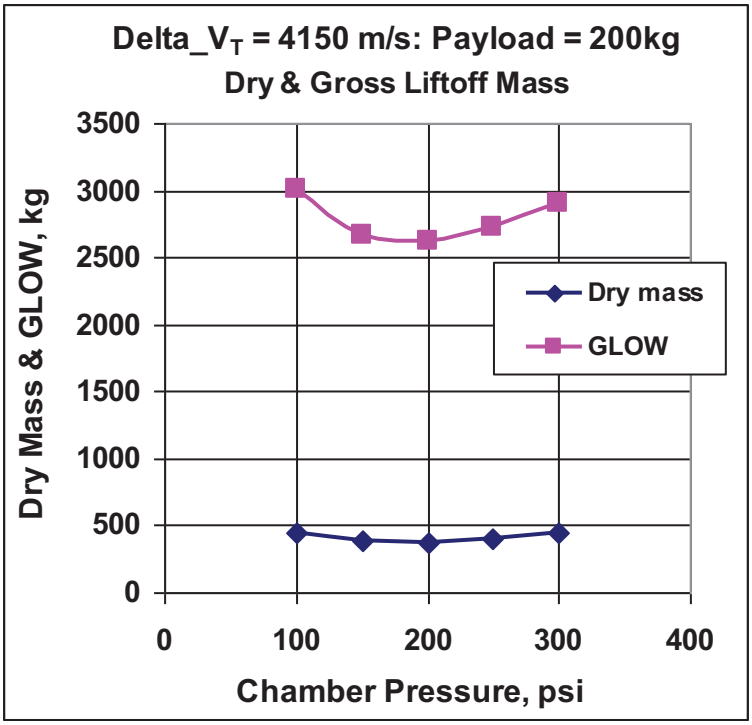


Figure 8.2.5 GLOW and dry mass versus chamber pressure

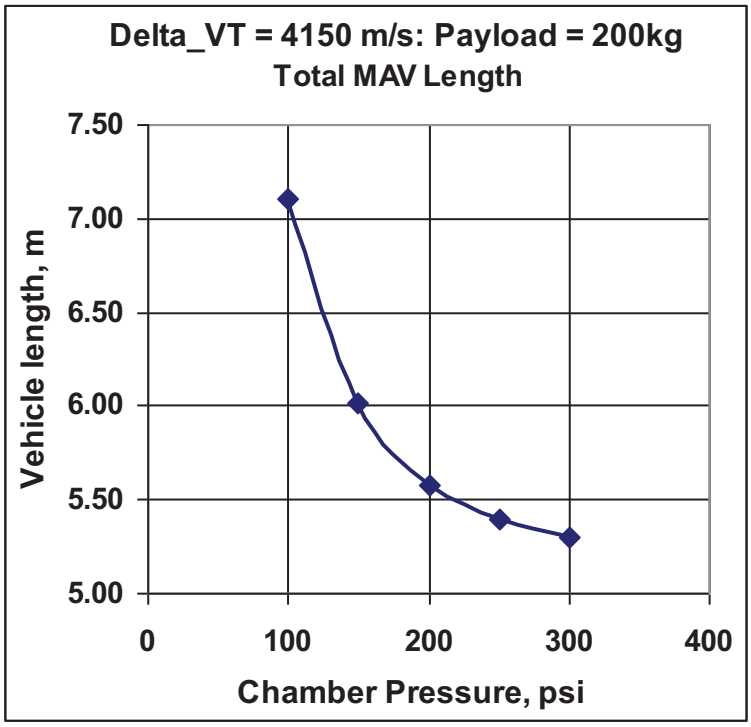


Figure 8.2.6 Vehicle overall versus chamber pressure

Table 6. 200 kg Payload mass pump feed versus pressure feed system comparison

	Pump Feed	Pressure Feed
Tank Pressure	0.034 MPa (5.0 psi)	1.72 MPa (250 psi)
Tanks	22.37 kg (18.8% Dry)	96.71 kg (33.2% Dry)
Structure	42.54 kg (35.9% Dry)	125.2 kg (43.0% Dry)
Main Engine	39.91 kg (33.7% Dry)	108.5 kg (37.3% Dry)
Pressurization	2.84 kg (2.4% Dry)	23.36 kg (8.0% Dry)
Main Propulsion	49.31 kg (41.6% Dry)	133.2 (45.8% Dry)
Dry Mass	154.1 kg (10.4% GLOW)	378.1 kg (14.4% GLOW)
Propellant Fraction	71.3%	73.1%
GLOW	1484 kg	2630 kg
Length	3.95 m	5.58 m
Diameter	0.909 m	1.044 m

8.3 Cryogenic Propellant Trade

The baseline propellant system is space storable hypergolic propellant with a turbo-pump feed engine. A trade study was conducted to examine the impact of going to storable/cryogenic or all cryogenic propellants. Appendix B presents the engine performance comparison various storable and cryogenic propellants (Figure B2). Table 7 compares the physical properties for various hydrocarbon and hypergolic fuel/oxidizer mixtures. From an engine performance perspective, the methane/liquid oxygen combination provides the best engine performance and was selected for the trade study. RP-1/LOX has a lower engine specific impulse (about 4%), but has a bulk propellant density roughly 25% higher than the methane/liquid oxygen combination, and was also selected for study.

Using the XLR-132 as the baseline engine and the 1-D rocket performance code, the hypergolic engine has an engine specific impulse of 343 seconds, compared to approximately 370 seconds for the methane/liquid oxygen combination at the baseline engine chamber pressure and nozzle expansion ratio. The higher engine specific impulse will result in a lower fuel fraction required, however the lower aggregate propellant density will result in a larger vehicle to contain the propellant. The choice of the cryogenic fuels will also introduce design issues associated with the low temperature propellants. Transient heat transfer analysis indicated that 1.0 inch of a low-density rigid cryogenic insulation would prevent the external wall temperature from reaching the condensation temperature of the atmospheric carbon dioxide for approximately 15 minutes.

The RP-1/LOX engine provides 354 seconds of engine specific impulse based on the 1-D rocket performance code, compared again to 343 seconds for the storable hypergolic propellants, and has a similar bulk propellant density to the hypergolic propellants.

Table 8 presents a comparison between the hypergolic and selected cryogenic propellants for a 200 kg payload mass and a total ΔV of 4150 m/sec. Comparisons are also made for a single engine and a 3 engine configuration. Engine nozzle expansion ratio was optimized for minimum gross liftoff mass. Due to lower propellant density for the methane/liquid oxygen design, the fore-body fineness ratio was increased to reduce overall vehicle length, but does not violate the maximum allowed body diameter limit of 1.2 m. For the RP-1/LOX design, the fore body diameter-to-length ratio was optimized for minimum gross liftoff mass. Table 9 presents a more detailed mass comparison for the various propellant combinations.

The propellant fraction is lower for the methane/liquid oxygen propellant combination, due to the higher engine specific impulse noted above. For the closed designs, the overall length of the cryogenic vehicle is similar to than that of the higher density hypergolic propellant, due mainly to closing at a lower gross liftoff mass and higher diameter-to-length ratio. The dry mass of the methane/liquid oxygen vehicle is higher compared to the storable propellant design, due to higher surface area and required cryogenic tank insulation. The closed gross liftoff mass is slightly lower for the methane/liquid oxygen propellant concept, by roughly only 4%. The RP-1/LOX vehicle exhibits higher dry mass, but lower gross mass compared to the hypergolic propellant design.

The propellant trade study was also repeated for the C_3=0 architecture. Table 10 presents a comparison between the hypergolic and selected cryogenic propellants for a 120 kg payload mass and a total ΔV of 5500 m/sec. Similar trends are found as for the lower total ΔV mission, with the methane/liquid oxygen concept having a higher dry mass of nearly 23%, but a slightly lower gross liftoff mass, on the order of roughly 5%. The RP-1/LOX vehicle shows 10% higher dry mass and 3% lower gross mass.

The gross and dry mass of the MAV vehicle is driven largely by the performance and weight characteristics of the rocket engine. By far, the performance parameter that has the biggest impact on the vehicle design is the engine specific impulse, regardless of propellant choice. Figures 8.3.1 through 8.3.3 present vehicle gross mass, dry mass and overall length sensitivity to engine specific impulse for the orbital architecture. For all studied propellant concepts, a1% change in specific impulse results in a 2% change in gross liftoff mass and 1% change in dry mass and vehicle length. The methane/oxygen vehicle shows a slightly higher sensitivity of the overall vehicle length to engine performance. Figures 8.3.4 through 8.3.6 present the gross mass, dry mass and overall vehicle length sensitivity as a function of the relative rocket engine mass. Gross liftoff mass and vehicle length have similar sensitivities for all propellant combinations. Vehicle dry mass shows the highest sensitivity to engine mass, but less than "one-for-one" in growth sensitivity. The storable hypergolic propellant design exhibits the largest dry mass sensitivity to engine mass variations.

The cryogenic propellant designs offer the possibility of modest reduction in gross liftoff mass, with increase in dry mass on the order of 10% for the RP-1/LOX configuration and 20% for the CH4/LOX design for total ΔV mission requirements of 4150 and 5500 m/sec. The use of in-situ resource utilization (ISRU) offers the potential of significant reduction on landed MAV mass, with one or both of the propellants being produced and stored on Mars. For the RP-1/LOX configuration, MAV landed mass can be reduced 50% for the orbital architecture, and to 60% for the C_3=0 architecture. The CH4/LOX concept would provide even higher MAV landed mass (70% to 80%) savings, since both propellants could be produced on the surface of Mars. The total landed weight savings must of course account for the mass, power and volume required by the additional subsystems to produce and store cryogenic propellants on the Martian surface.

Table 7. Propellant properties

Fuel	Oxidizer	Mol Wt	Density (kg/m^3)	O/F_S & O/F_{Opt}	Prop Density @ O/F_{Opt}	B.P (^oK)	V.P @ Room Temp (bars)	Comb Temp (^oK)
CH_4	LOX	16	423	4.0/3.0	800.7	111.4	58	3419
C_3H_8	"	44	582	3.6/3.0	920	231	8.5	3577
C_4H_{10}	"	58	601	3.57/3.0	932	272	1.0	3592
C_5H_{12}	"	72	621	3.55/3.0	943	309	.579	3601
C_8H_{18}	"	114	703	3.50/3.0	987	399	.0147	3613
RP-1	"	~175	807	3.4/2.25	1012	422	.020	3497
C_2H_5OH	"	46	789	2.08/1.70	979	352	.0595	3352
N_2H_4	NTO	32	1021	1.44/1.25	1218	387	.010	3263
MMH	'	46	875	2.56/1.96	1185	364	.050	3387
UDMH	'	60	790	2.613.06	1175	337	.137	3472

Table 8. Orbital/200kg payload hypergolic and cryogenic performance comparison

	MMH/NTO		RP-1/LOX		CH4/LOX	
No. Engines	1	3	1	3	1	3
Opt ε	200	200	175	200	200	225
Opt D/L_{FB}	0.3125	0.3125	0.3516	0.3516	0.3906	0.3906
Propellant Fraction	0.715	0.714	0.700	0.699	0.685	0.684
Length	3.95	3.55	3.86	3.52	3.91	3.56
Diameter	0.909	0.914	0.996	1.004	1.093	1.103
Dry Mass	154.1	145.8	165.6	159.4	182.5	176.0
Dry Mass %	10.38	10.10	11.44	11.25	12.81	11.51
GLOW	1484	1450	1448	1417	1425	1397

Table 9. Orbital/200kg comparison between hypergolic and cryogenic propellants

Propellants	**MMH/NTO**	**RP-1/LOX**	**CH4/LOX**
Engine Thrust, N	**13802**	**13468**	**13253**
Engine Thrust-to-Weight	**35.2**	**35.62**	**34.70**
Engine Mass, kg	**39.9**	**38.51**	**38.90**
Fuel/Oxidizer Volume, m^3	**0.429/0.508**	**0.406/0.738**	**0.695/0.769**
Fuel Tank Mass, m	**10.73**	**10.22**	**16.11**
Oxidizer Tank Mass, m	**11.64**	**17.23**	**17.86**
Tank Insulation Mass. kg	**0.0**	**3.84**	**8.49**
Structure, kg	**42.54**	**48.97**	**55.81**
Propellant Feed & Press Mass, kg	**2.84**	**3.12**	**3.65**
Main Propulsion Mass	**49.31**	**48.04**	**48.98**
Thrust Structure mass, kg	**4.65**	**4.86**	**5.13**
Prime Power Mass, kg	**2.33**	**2.28**	**2.25**
Power Conversion & Dist Mass, kg	**3.52**	**3.52**	**3.56**
Propellant Feed System mass, kg	**1.33**	**1.37**	**1.52**
Engine Gimbal/Control mass, kg	**5.80**	**5.67**	**5.71**
Dry Mass, kg	**154.06**	**165.60**	**182.52**
Propellant Mass, kg	**1119.23**	**1072.12**	**1032.83**
Overall Body Length / Diameter, m	**3.95 / 0.909**	**3.86/0.996**	**3.91/ 1.093**
GLOW, kg	**1484**	**1448**	**1425**
Propellant Fraction Available, %	**71.3**	**70.0**	**68.5**

Table 10. C3=0/120kg comparison between hypergolic and cryogenic propellants

Propellants	MMH/NTO	RP-1/LOX	LOX/CH4
Engine Thrust, N	20163	19531	19255
Engine Thrust-to-Weight	41.0	40.6	40.1
Engine Mass, kg	50.11	49.09	48.5
Fuel/Oxidizer Volume, m^3	0.711/0.841	0.669/1.194	1.132/1.254
Fuel Tank Mass, m	16.67	15.81	24.56
Oxidizer Tank Mass, m	18.19	26.28	27.42
Tank Insulation Mass. kg	0.0	5.66	12.11
Structure, kg	52.74	61.85	72.00
Propellant Feed & Press Mass, kg	4.04	4.45	5.26
Main Propulsion Mass	62.36	61.26	61.45
Thrust Structure mass, kg	6.39	6.66	7.07
Prime Power Mass, kg	3.22	3.13	3.09
Power Conversion & Dist Mass, kg	3.66	3.67	3.71
Propellant Feed System mass, kg	1.79	1.85	2.05
Engine Gimbal/Control mass, kg	6.73	6.64	6.59
Dry Mass, kg	179.14	197.54	220.02
Propellant Mass, kg	1853.2	1766.9	1715.0
Overall Body Length / Diameter, m	4.38 / 0.993	4.34/1.090	4.39/ 1.207
GLOW, kg	2168	2100	2070
Propellant Fraction Available, %	80.9	79.6	78.4

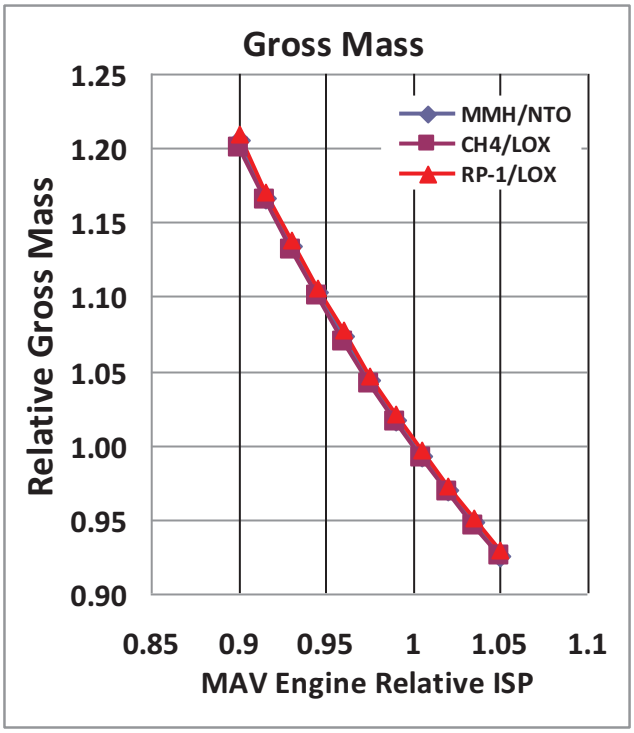


Figure 8.3.1 Relative gross liftoff mass versus relative engine specific impulse

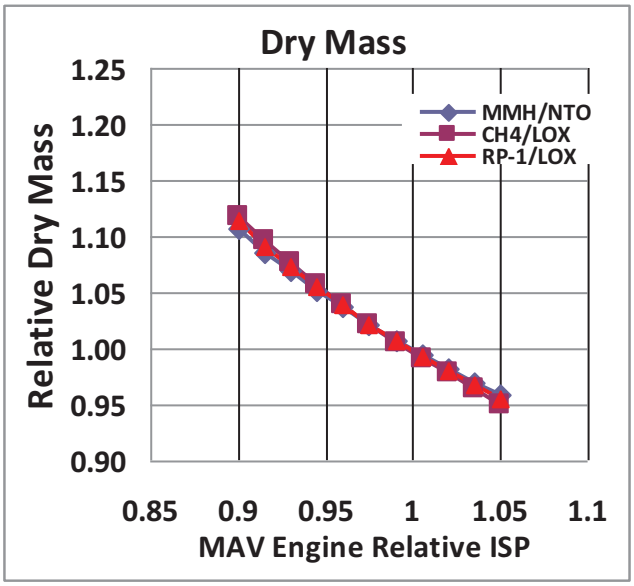


Figure 8.3.2 Relative dry mass versus relative engine specific impulse

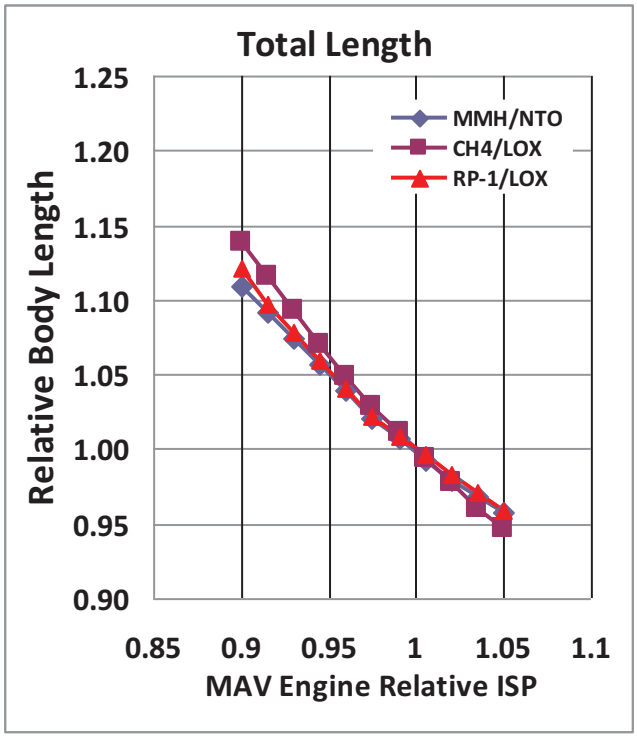


Figure 8.3.3 Relative vehicle length versus relative engine specific impulse

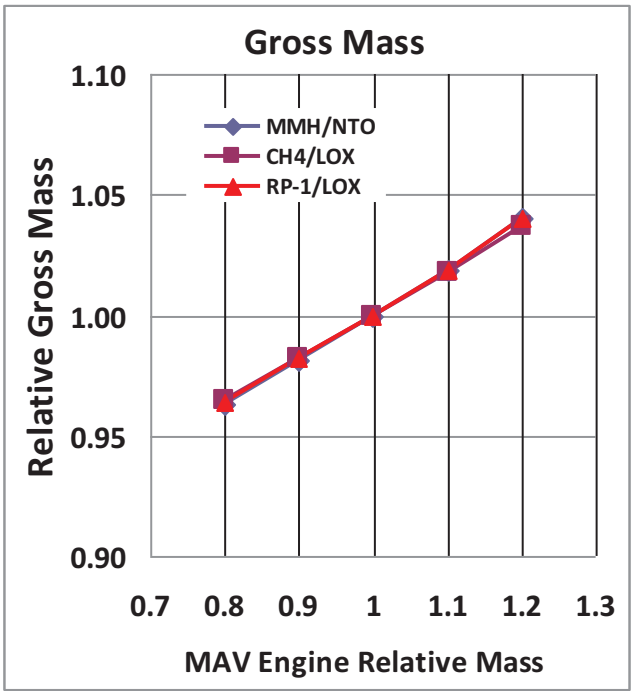


Figure 8.3.4 Relative gross liftoff mass versus relative engine mass

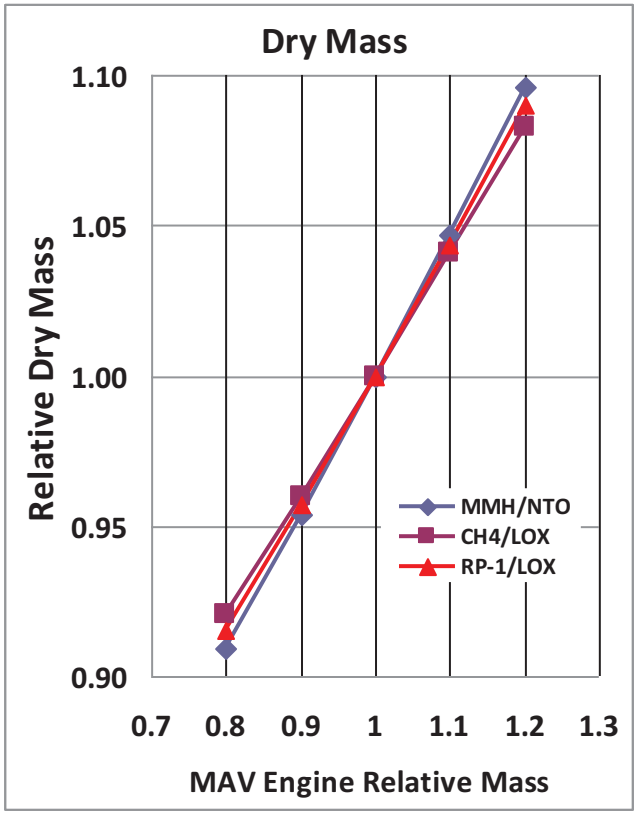


Figure 8.3.5 Relative dry mass versus relative engine mass

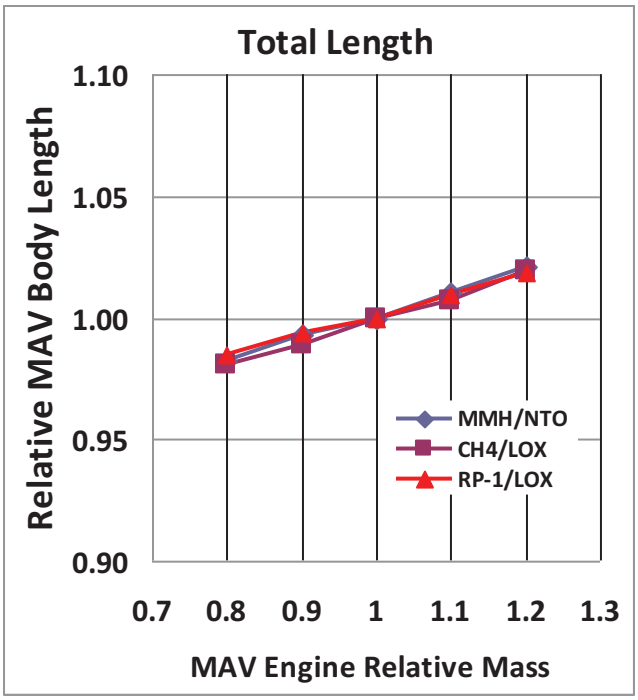


Figure 8.3.6 Relative overall vehicle length versus relative engine specific mass

9.0 Final Configurations

During the course of this MAV conceptual design and technology requirements study, a concurrent effort focused on the conceptual design of the ERV, including total ΔV requirements and two propulsion systems options: 1) all chemical propulsion and 2) solar-electric propulsion. Two ERV designs evolved and preliminary mass and scale estimates were provided to the MAV design team. For the chemical propulsion ERV, an optimal ΔV split of 50% MAV and 50% ERV was determined and the associated mass and volume of the ERV defined. The MAV design closure process was repeated for the two finalized ERV concepts and the results presented here, along with the pressure-feed 20kg inert payload mass MAV design. Table 11 presents a MEL weight statement and overall vehicle dimensions for the three MAV configurations. All concepts utilize storable hypergolic propellants.

9.1 Inert Capsule to low Mars orbit rendezvous

For the 20kg inert capsule Mars orbit rendezvous architecture, a pressure-feed single engine concept was selected for the final design. The decision to go with pressure-feed engine was driven in part by the large down scaling range required for the baseline turbo-pump feed engine. The second column of Table 11 presents the MEL mass statement for the inert capsule MAV, including subsystem mass and dry mass or gross mass fraction. The high pressure propellant tanks dominate the total structural mass, with a dry mass fraction of 27%. Total dry mass is 64.7 kg, which is 17% of the gross liftoff mass. Total propellant mass fraction is77.4%, which includes ascent propellant, reserves and engine start-up. The payload mass fraction is 5%, with a gross liftoff mass of 393 kg. The overall vehicle length is 2.74 meters and diameter of 0.56 meters.

9.2 Optimized ΔV Split Architecture

For the chemical propulsion ERV, the MAV total ΔV is 4250 m/sec and the ERV mass is 230 kg, with a volume of 0.575 m^3. The engine design is turbo pump-feed, 3 engine configuration

with a engine nozzle expansion ratio of 200. For the low pressure propellant tank concept, the structural dry mass fraction is 40% and the main propulsion system dry mass fraction is 39%. Total dry mass is 165 kg, which is ~10% of the gross liftoff mass. Total propellant mass fraction is76.3%, which includes ascent propellant, reserves and engine start-up. The payload mass fraction is 13.4%, with a gross liftoff mass of 1719 kg, below the estimated landed mass limit. The overall vehicle length is 3.75 meters and diameter 0.97 meters, also below the length and diameter constraints.

9.3 SEP Architecture

For the SEP ERV, the MAV total ΔV is 5500 m/sec and the ERV mass is 110 kg, with a volume of 0.275 m^3. The engine design is turbo pump-feed, single engine configuration with a engine nozzle expansion ratio of 200. The structural dry mass fraction is 38% (tank dry mass fraction is 25%) and the main propulsion system dry mass fraction is 46%. Total dry mass is 170 kg, which is 8.4% of the gross liftoff mass. For the C_3=0 mission, the total propellant mass fraction is 85.5%, which again includes ascent propellant, reserves and engine start-up. The payload mass fraction is 5.4%, with a gross liftoff mass of 2025 kg, very close to the estimated landed mass limit. The overall vehicle length is 4.28 meters and diameter 0.97 meters.

Trade studies on the number of engines (Section 8) suggest a reduction in gross liftoff mass on the order of 5% can be achieved by going to a multi-engine configuration. The GLOW of the SEP architecture MAV could possibly be reduced to roughly 1900 kg, leaving only 100 kg for other landed payload elements. Application of the cryogenic propellant could also provide further GLOW reduction. The vehicle length exceeds the landing capsule length constraint. Initial design sensitivity trade studies indicated low gross liftoff mass sensitivity to fore body diameter-to-length ratio. The fore body fineness are could therefore be increased to reduce the overall vehicle length to meet the 4.0 meter length constraint, and meet the maximum diameter limit with modest gross liftoff mass increase.

Table 11. Final concepts mass statement and dimensions

ERV Concept	Inert	Chemical Prop	SEP
ΔV_{TOTAL}/ERV Mass	4150 / 20 kg	4250 / 230 kg	5500 / 110 kg
Total Structure, kg (% Dry Mass)	18.33 (36.8%)	51.76 (40.8%)	49.61 (37.9%%)
Aft Compartment + Secondary	0.85 (1.7%)	2.76 (2.2%)	2.17 (1.6%)
Tanks	13.29 (26.7%)	25.71 (20.5%)	32.96 (25.1%)
Thrust Structure	1.96 (3.9%)	7.77 (6.1%)	6.02 (4.6%)
Payload Adapter	1.05 (2.1%)	12.07 (9.5%)	5.77 (4.4%)
Aeroshell	1.18 (2.4%)	3.44 (2.7%)	2.67 (2.0%)
Induced Environments	2.10 (4.0%)	2.68 (2.1%)	4.64 (3.5%)
Auxiliary (Separation) Systems	2.61 (5.2%)	18.67 (14.7%)	9.49 (7.2%)
Main Propulsion	22.3 (44.8%)	48.82 (38.5%)	59.59 (45.5%)
Main Engine(s)	18.76 (37.7%)	44.87 (35.4%)	48.17 (36.8%)
Feed & Pressurization	3.34 (6.7%)	3.07 (2.4%)	3.82 (2.9%)
Engine Control, Purge & Install	0.20 (0.4%)	0.87 (0.7%)	7.6 (5.8%)
Prime Power	0.40 (0.8%)	0.40 (0.3%)	3.05 (2.3%)
Power Conversion/Distribution	3.12 (6.3%)	3.49 (2.8%)	3.63 (2.8%)
DHCC	1.0 (2.0%)	1.0 (0.8%)	1.0 (0.8%)
Contingency	14.93 (30%)	38.05 (30%)	39.3 (30%)
Dry Mass, kg (%GLOW)	64.72 (16.5%)	164.88 (9.6%)	170.3 (8.4%)
Propellants, kg (%GLOW)	303.88 (77.4%)	1311 (76.3%)	1740 (85.5)
Residuals + Pressurants, kg (%GLOW)	3.85 (0.1%)	12.48 (0.7%)	15.4 (0.7%)
Payload, kg (%GLOW)	20 (5.1%)	230 (13.4%)	110 (5.4%)
Gross Liftoff Mass, kg	392.6	1719	2035
Engine(s) and Thrust/Engine	3 / 1210 nts	3 / 5330 nts	1 / 18,925 nts
Overall length/Diameter, m	2.74 / 0.56	3.75 / 0.97	4.28 / 0.97

10.0 Conclusions & Recommendations

A preliminary study was conducted to assess the impact of mission requirements and technology performance on the mass and size of various classes of Mars Ascent Vehicles, limited by allowable mass and volume of the landing capsule. Trade studies were completed to define vehicle mass and scale sensitivity to engine/propellant type and configuration, fore body geometry, payload mass and total ΔV requirements.

The volume/length constraints imposed on the MAV design resulted in a single stage-to-orbit architecture, and in turn the requirement for high performance, high thrust-to-weight rocket engine. A high pressure turbo pump-feed, high expansion ratio engine utilizing storable hypergolic propellants was selected for the baseline main propulsion engine, with engine specific impulse of 340+ seconds and an engine thrust-to-weight ratio of 30+. A nested tank design was chosen to eliminate the fuel/oxidizer inter-tank section, saving weight and reducing overall vehicle length. Composite materials were selected for tanks, aft compartment and aeroshell construction based on potential weight savings. Aerodynamic and aerothermal considerations do not significantly impact MAV performance and closure mass.

For the inert 20 kg class payloads to low Mars rendezvous orbit, a pressure-feed hypergolic engine easily meets the down mass and volume constraints imposed by the landing capsule. A pump-feed concept has lower gross liftoff mass, however scaling of the baseline engine to meet thrust-to-weight requirements resulted in an engine size only ~15% of the baseline engine. The

engine performance and mass scaling models may not accurately reflect engine performance at that scale.

For propulsive ERV concepts in the 100 to 200+ kg mass class, the pump-feed engine concept is enabling technology. Pressure-feed concepts are not competitive and significantly exceed mass and volume constraints. For the optimal ΔV split architecture, storable hypergolic and all cryogenic methane/oxygen and kerosene/liquid oxygen concepts are equally competitive, with a slight gross mass edge for the cryogenic systems and a lower dry mass for the hypergolic design. The C_3=0 baseline architecture marginally meets the mass and vehicle length constraints, but would leave little mass availability of other mission systems. The overall impact of ISRU technology needs to be assessed, with the mass, power and volume requirements by the additional subsystems to produce and store cryogenic propellants on the Marian surface determined, balanced against potentially significant mass saving in the landed MAV mass.

Engine performance and mass characteristics have the biggest impact on the MAV design. The availability of a high performance, low mass turbo pump-feed engine in the proper thrust size is critical for the ERV class missions. The application of accurate engine performance and mass estimation models are highly recommended to confirm and refine the present conceptual design performance predictions. The mass estimating relationships used in the vehicle closure process for critical subsystems were based on much larger scale launch vehicles and often resulted in extrapolation of the design data base. More physics-based analysis is also recommended for further preliminary design efforts for the MAV concepts. Finally, a refined estimate of the landed payload capability of the entry capsule is recommended to assess the viability of the SEP ERV architecture.

Appendix A: Engine Trades

A quasi-one dimensional rocket performance code was developed to predict engine performance as a function of chamber pressure, oxidizer-to-fuel ratio and nozzle expansion ratio. The equilibrium thermo-chemical model is based on the NASA Glenn CEA code (Reference 10), with addition subroutines developed to predict the thermodynamic properties of the nozzle flow assuming fixed mole fractions, i.e. frozen flow. The mass, momentum and energy equations are solved over a finite area ratio control volume. Based on published engine performance characteristics, the best match to the engine performance was obtained assuming frozen flow starting at the nozzle throat.

For a mixture of hypergolic propellants, specifically MMH and NTO, the predicted engine performance, namely engine specific impulse and thrust per unit nozzle exit area is presented in Figures A1 and A2, respectively. The oxidizer-to-fuel ratio has been optimized to produce maximum engine specific impulse, and has a fuel-rich value of 2.0. As presented in Figure A1, engine specific impulse increases with both increasing nozzle expansion ratio and increasing thrust chamber pressure. Thrust per unit nozzle exit area is a nearly linear function of chamber pressure, and decreases with increasing nozzle expansion ratio. For a required amount of rocket engine thrust, the thrust per unit nozzle exit area is an indicator of the physical size of the engine, with engine size varying roughly inversely with nozzle expansion ratio.

The reference engine selected was the Rocketdyne orbital-transfer XLR-132, a hypergolic, gas-generator, pump-feed engine. The chamber pressure is 10.34 MPa (1500 psi) and it has a nozzle expansion ratio of 400. The predicted performance of the engine is within 0.5% of both specific impulse and thrust per unit nozzle exit area. Weight scaling of the engine with expansion ratio was based on the XLR-132, with a nozzle unit mass of approximately 12.5 kg/m^2.

Using the XLR-132 as the baseline engine, trades on engine mass, thrust-to-weight characteristics and engine nozzle exit diameter as a function of expansion ratio and chamber pressure were conducted. For a fixed engine thrust of approximately 12,000 N, the engine mass, engine thrust-to-weight and nozzle exit diameter are presented in Figures A3 through A5. As both chamber pressure and nozzle expansion ratio are increased, engine mass and nozzle diameter decrease, while engine thrust-to-weight increase. For the expansion ratio = 100, a minimum in the engine weight occurs around 4.1 – 5.5 MPa (600 to 800 psi).

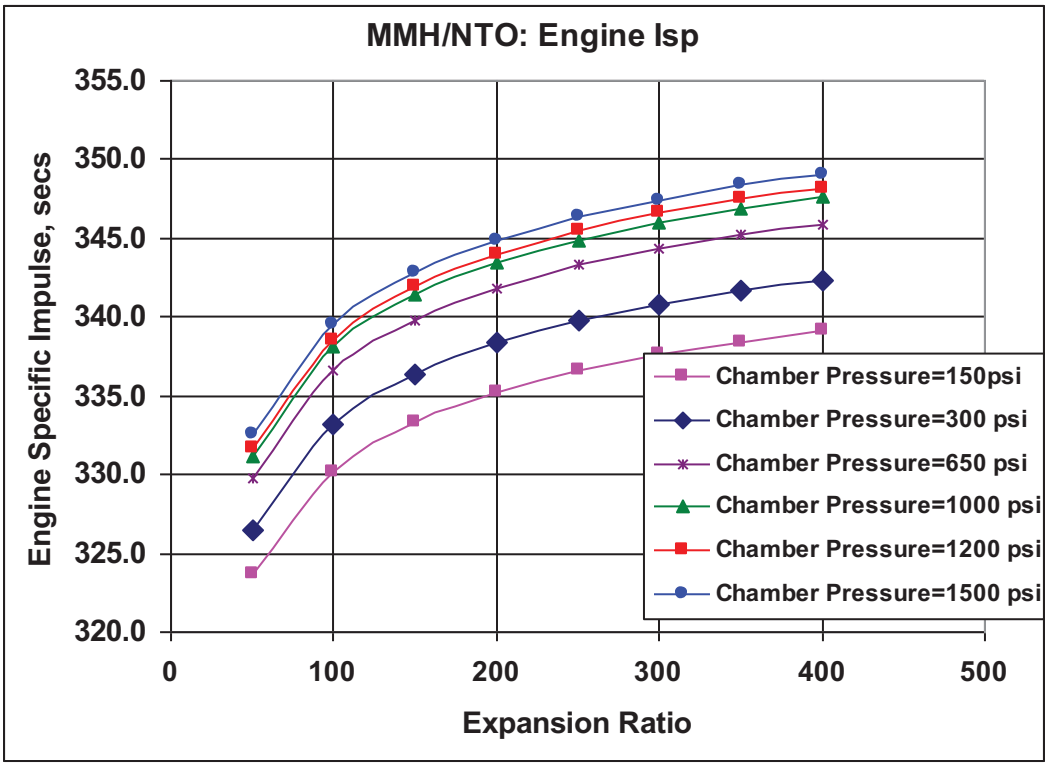


Figure A1. Engine specific impulse versus chamber pressure and nozzle expansion ratio.

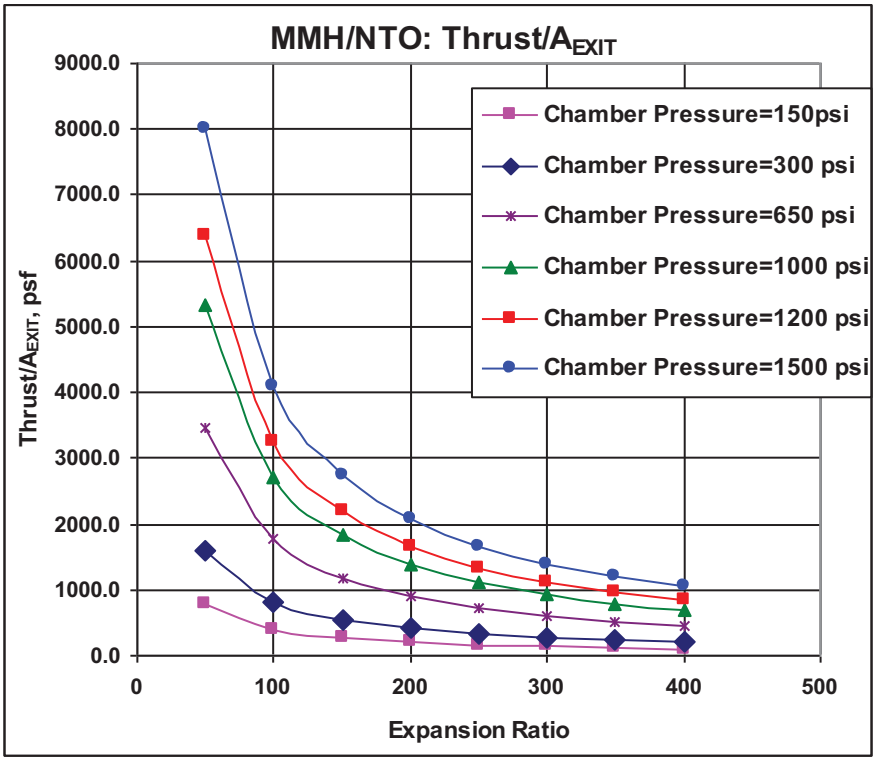


Figure A2. Engine thrust per unit nozzle exit area versus chamber pressure and nozzle expansion ratio.

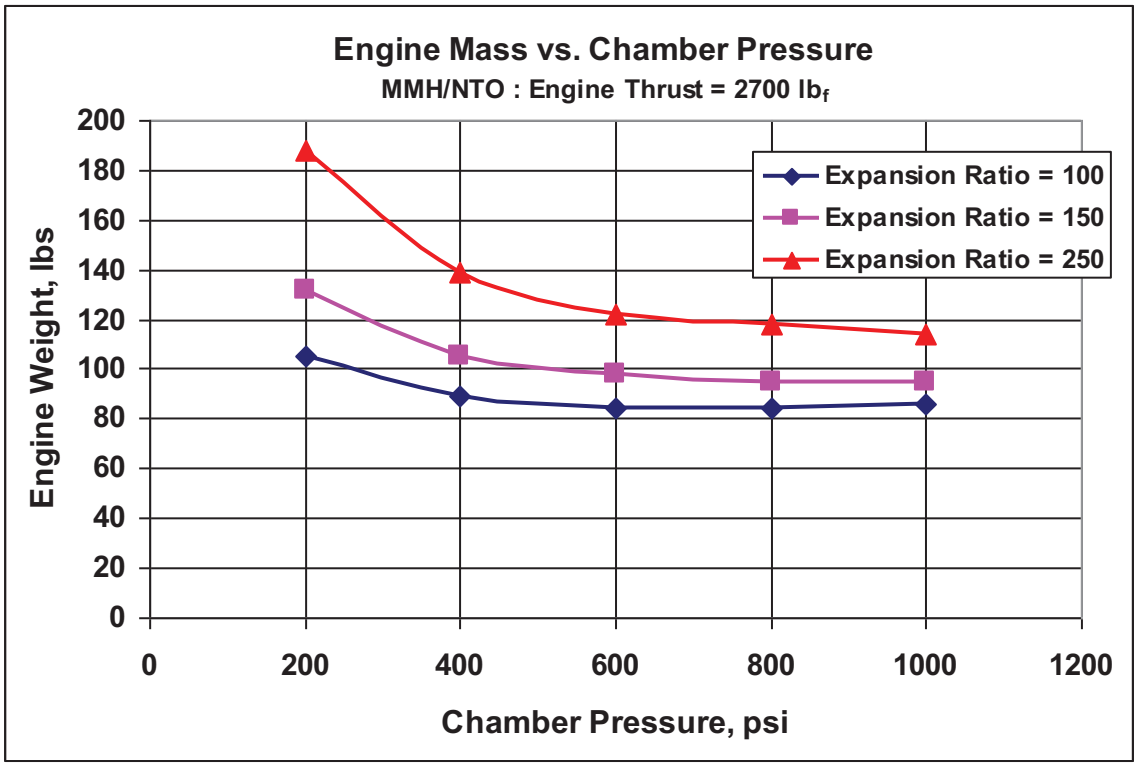


Figure A3. Engine mass versus chamber pressure and nozzle expansion ratio.

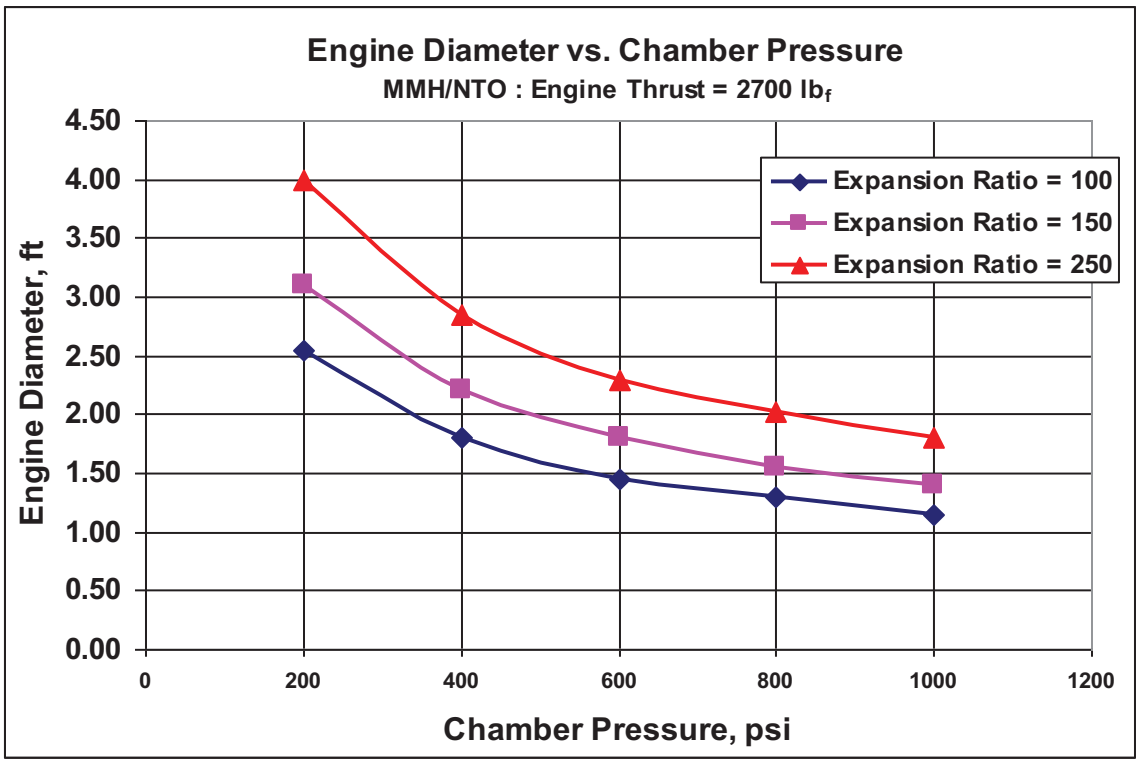


Figure A4. Engine diameter versus chamber pressure and nozzle expansion ratio.

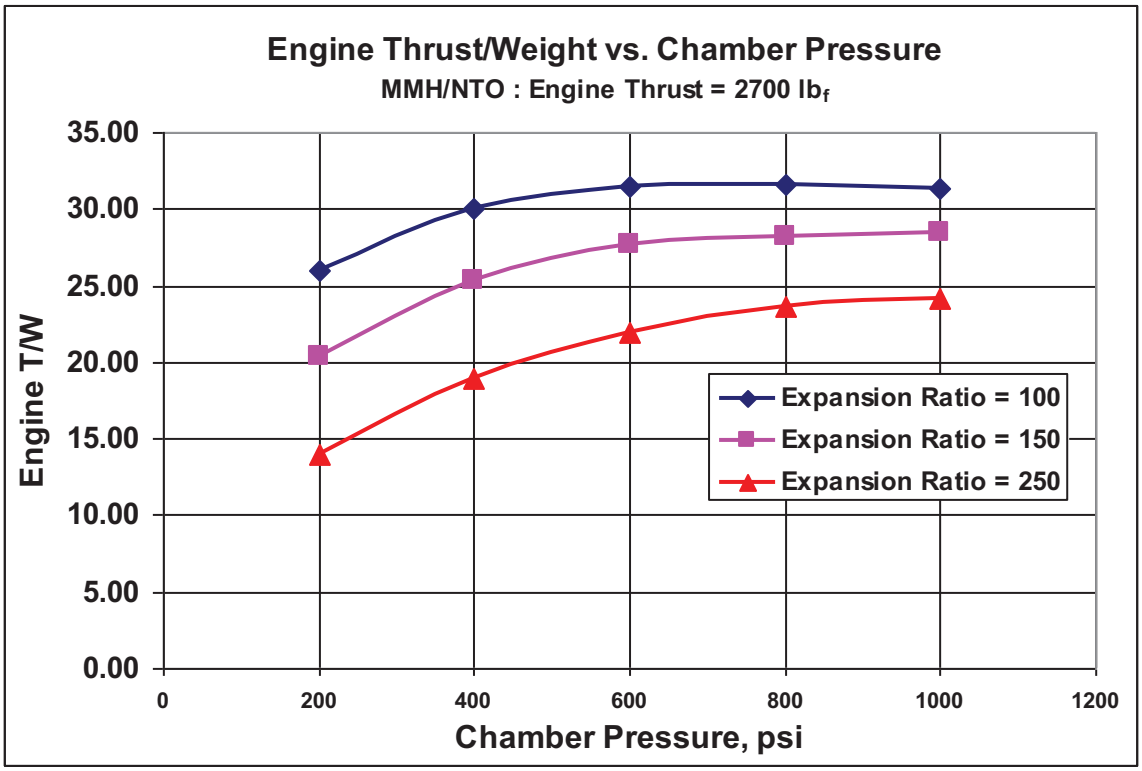


Figure A5. Engine thrust-to-weight versus chamber pressure and nozzle expansion ratio.

Appendix B: Propellant Trades

The baseline propellant selected was a storable hypergolic mixture of MMH and NTO. Alternate hypergolic fuels were also considered, including hydrazine and UDMH. Figure B1 shows the engine specific impulse for the three fuels with NTO at the optimum oxidizer-to-fuel mixture ratio as a function of nozzle expansion ratio. Although hydrazine has the highest specific impulse and the mean propellant density is similar for all three fuel/oxidizer combinations, MMH was selected as the baseline propellant because the reference engine (XLR-132) utilizes MMH and the predicted engine performance could be anchored to the actual engine performance.

Alternate hydrocarbon-based fuels with liquid oxygen were also considered. Figure B2 presents the engine specific impulse as a function of nozzle expansion ratio, at a chamber pressure of 4.48 MPa (650 psi) and an oxidizer-to-fuel mixture ratio of 3.0. Methane provides a significantly higher specific impulse compared to the higher molecular weight hydrocarbons and was selected as the fuel of choice for the hydrocarbon-based propellants. RP-1/LOX was also selected, based on mean propellant bulk density considerations. Engine performance of the RP-1/LOX design was based on an oxidizer-to-fuel ratio of 2.25.

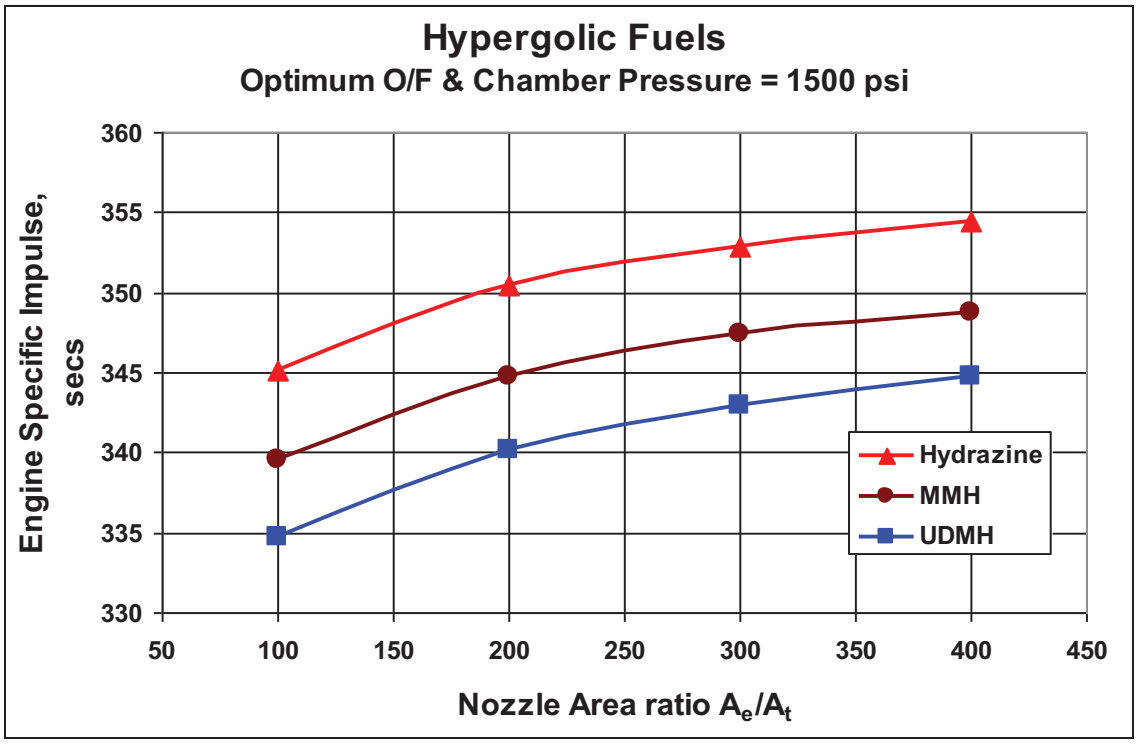


Figure B1. Engine specific impulse versus nozzle expansion ratio for various hypergolic fuels with NTO.

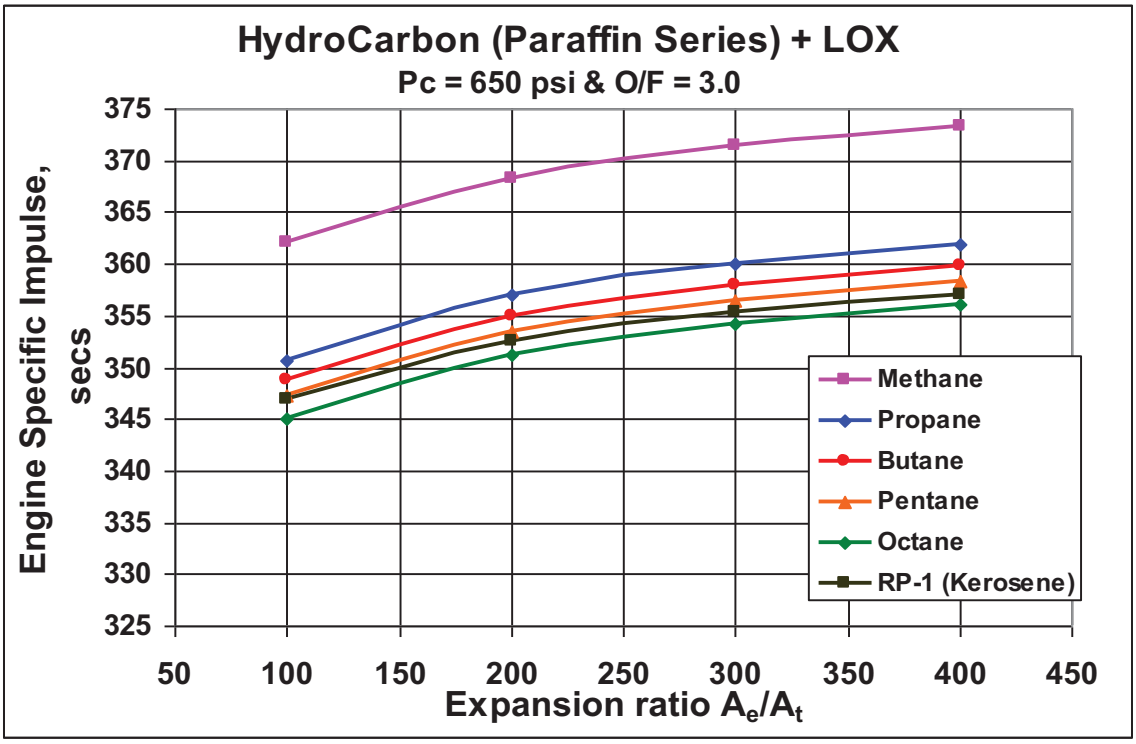


Figure B2. Engine specific impulse versus nozzle expansion ratio for various hydrocarbon fuels with liquid oxygen

Appendix C: CFD Solutions & Aeroheating

Cart3D was used to provide a preliminary aerodynamic analysis on the MAV vehicles. Cart3D solutions were computed for three candidate forebody shapes at subsonic, transonic and low supersonic flight conditions. Cart3D is a high-fidelity inviscid analysis package for conceptual and preliminary aerodynamic design. The adjoint mesh adaptive version of Cart3D was utilized allowing for a more automated set up of the inputs to the code and a more rapid arrival at reasonable solutions for a large range of flow conditions. Geometry is input via an unstructured triangular mesh elements with the option of tagging to denote different regions (ex. aerodynamic, propulsion, base etc...). Cart3D version v1.4.7_LINUX64—12.05.07 was used for the analysis in this report. The MAV Rev2 geometry was analyzed at Mach 0.5, 0.95, 1.05, 1.5 and 2.0 at four angles of attack (0°, 2°, 5° and 10°) with a typical solution running to over 1.5 million cells. Force and moment histories for each of the grid cycles was monitored for convergence quality for each case.

Figures C1 through C5 present Cart3D solutions at various Mach numbers and angles-of-attack, and show surface pressure coefficient distributions and Mach number contours.

Figure C6 summarizes the Euler solutions, plotting zero lift drag coefficient versus Mach number over the subsonic, transonic and low supersonic flight regimes. Figure C7 presents the pitching moment coefficient versus Mach number and angle-of-attack. For the selected moment reference (roughly 50% of body length), the vehicle is statically unstable in pitch. For the internal arrangement selected, with the oxidizer tank forward, the axial center-of-gravity shifts forward and the vehicle would be statically stable.

A preliminary trajectory was computed and the resulting Mach number, angle-of-attack and free-stream dynamic pressure history was used to interpolate the aerothermal database to estimate the ascent heating environment. Figures C8 and C9 summarized the heating environment, showing mission maximum heating rate distribution and mission integrated heat load, respectively. Peak heating occurs at roughly Mach = 5.0 and dynamic pressure of 60 Pa. Stagnation point peak heating is on the order of only 0.5 W/cm^2, and the integrated heat load is merely 0.5 MJ/m^2. Minimum gauge TPS on the nose cap region only (e.g. P-45 Cork) will be adequate. Peak acreage radiation equilibrium wall temperatures are on the order of 390ºK, well below allowable temperatures for the selected structural material.

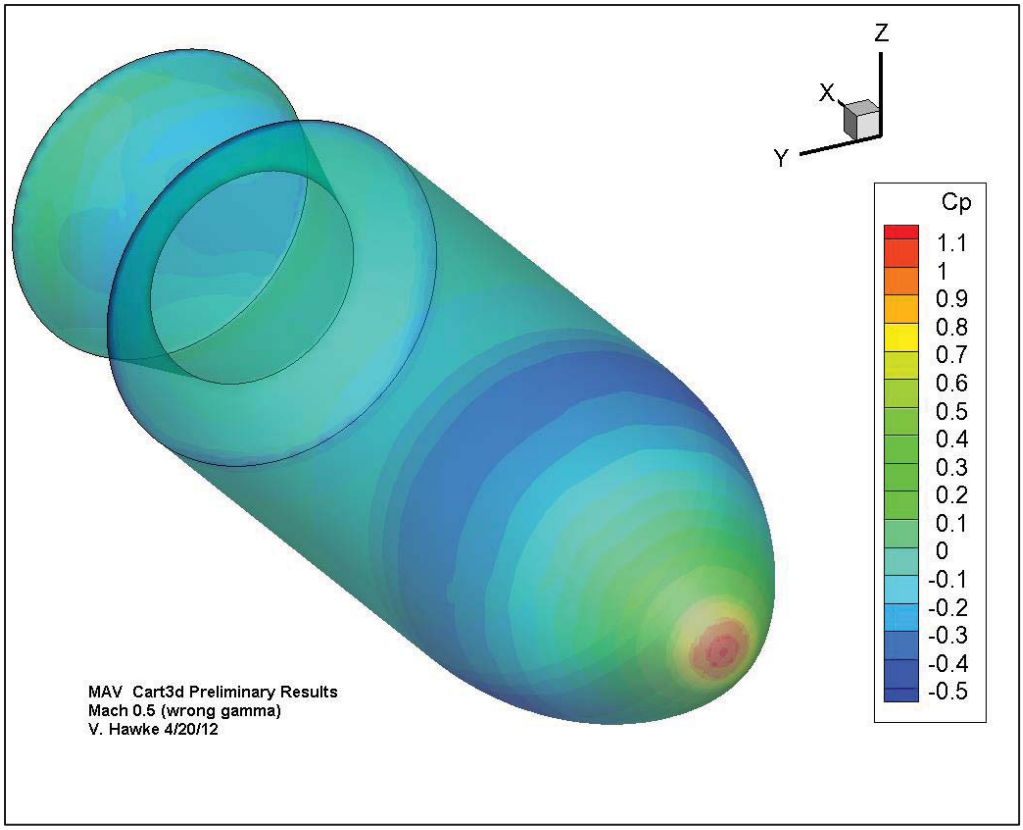


Figure C1. Cart3D predicted subsonic Mach = 0.6 surface pressure distribution for the Rev0 geometry

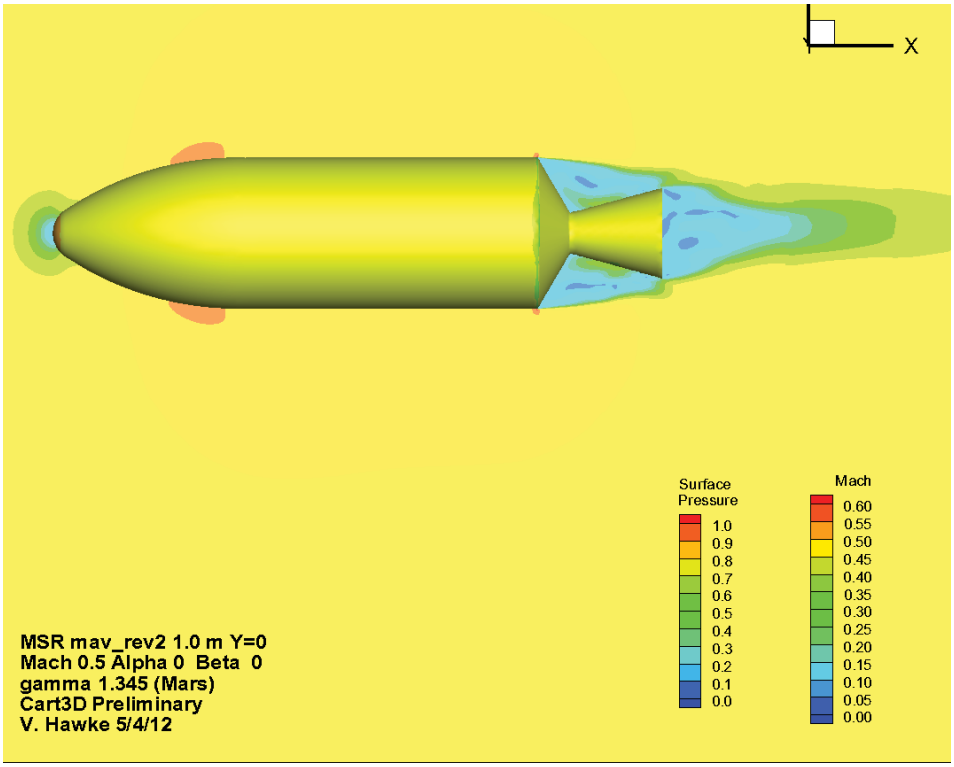


Figure C2. Cart3D predicted subsonic Mach = 0.5 surface pressure distribution and Mach number contours for the Rev2 geometry

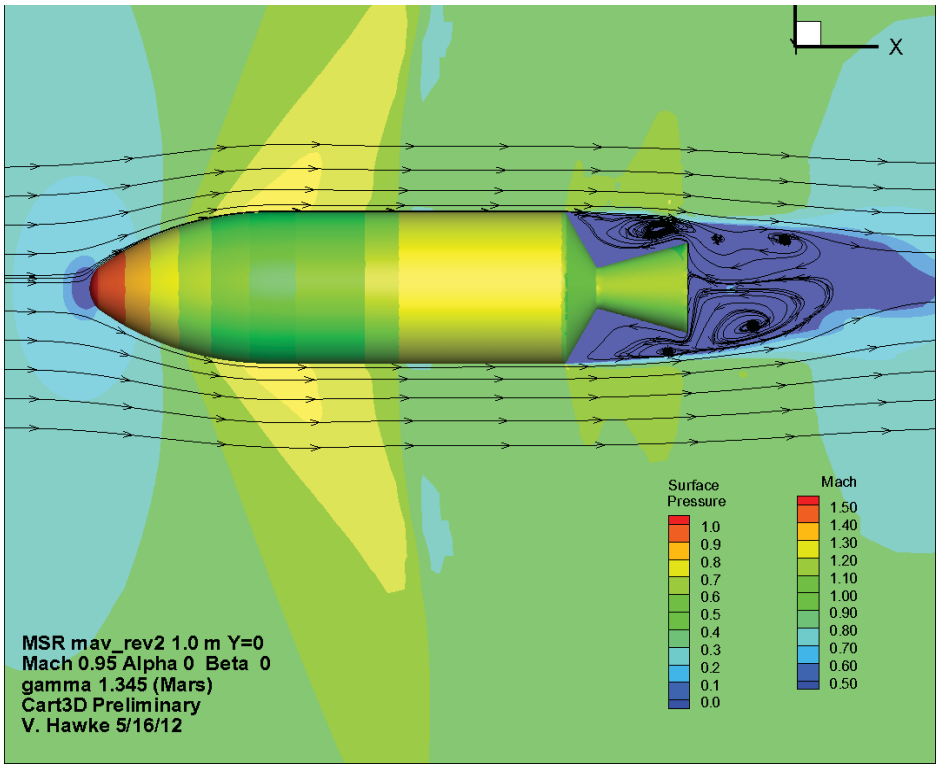


Figure C3. Cart3D predicted Mach = 0.95 surface pressure distribution and Mach number contours for the Rev2 geometry

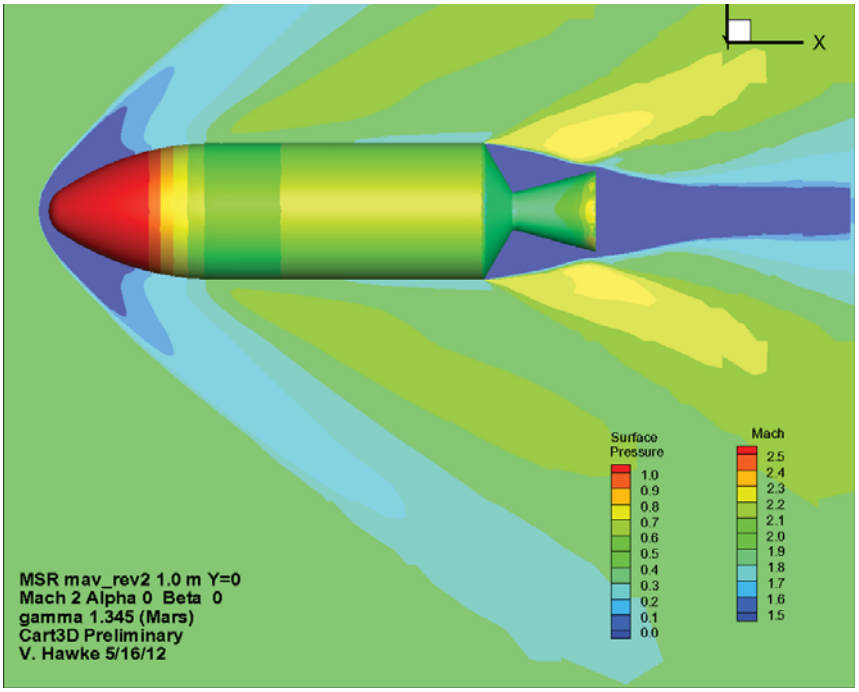


Figure C4. Cart3D predicted Mach = 2.0 surface pressure distribution and Mach number contours for the Rev2 geometry

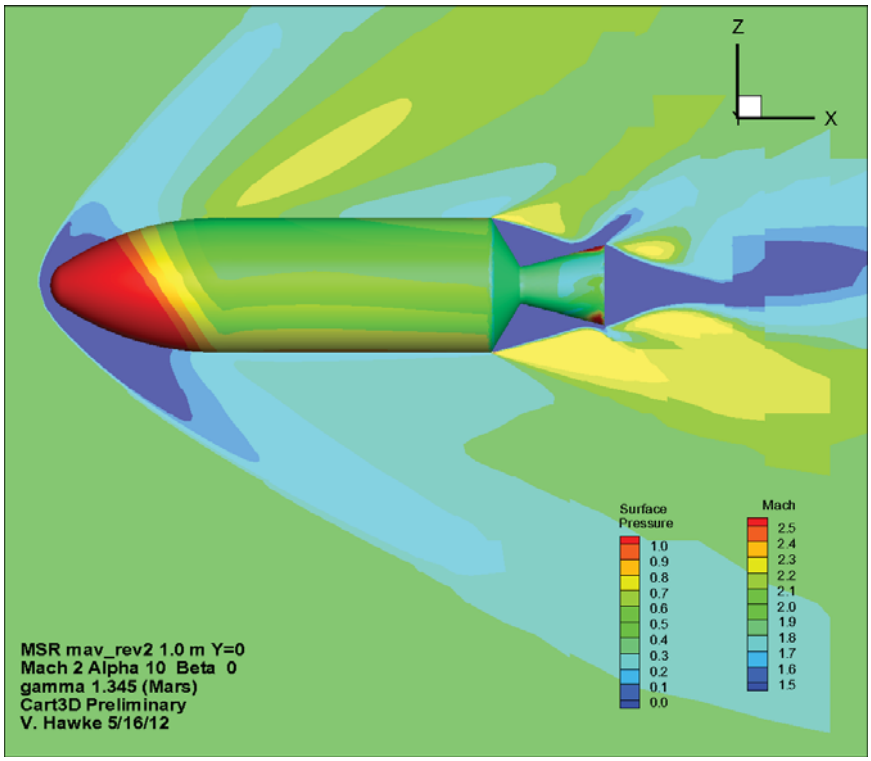


Figure C5. Cart3D predicted Mach = 2.0 and angle-of-attack = 10.0° surface pressure distribution and Mach number contours for the Rev2 geometry

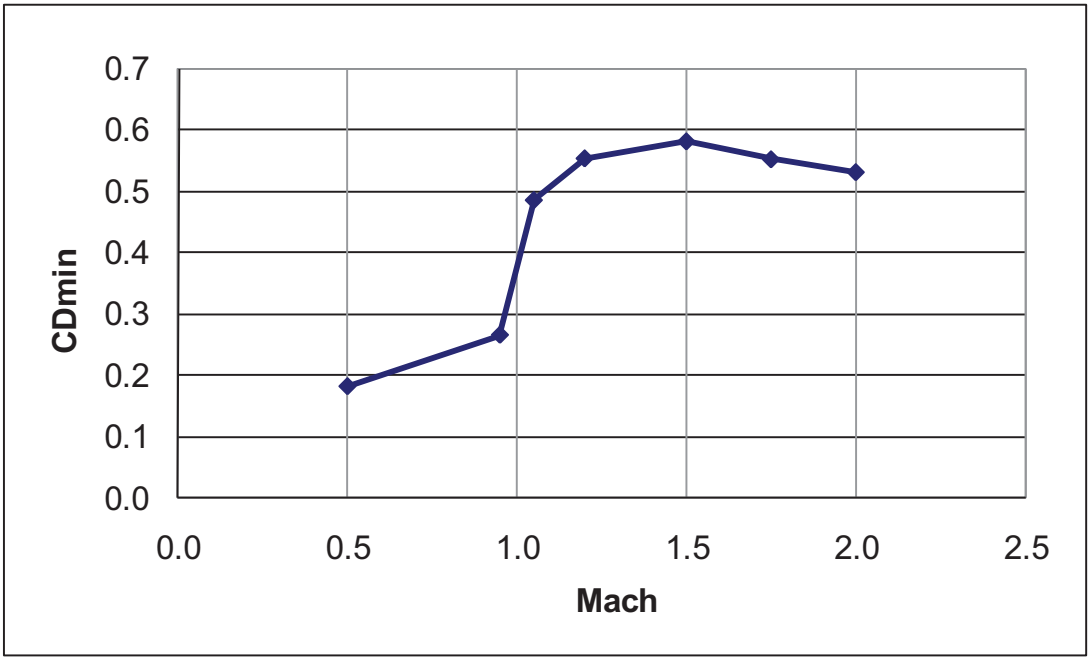


Figure C6. Zero-lift drag coefficient versus Mach number computed by CFD Euler code

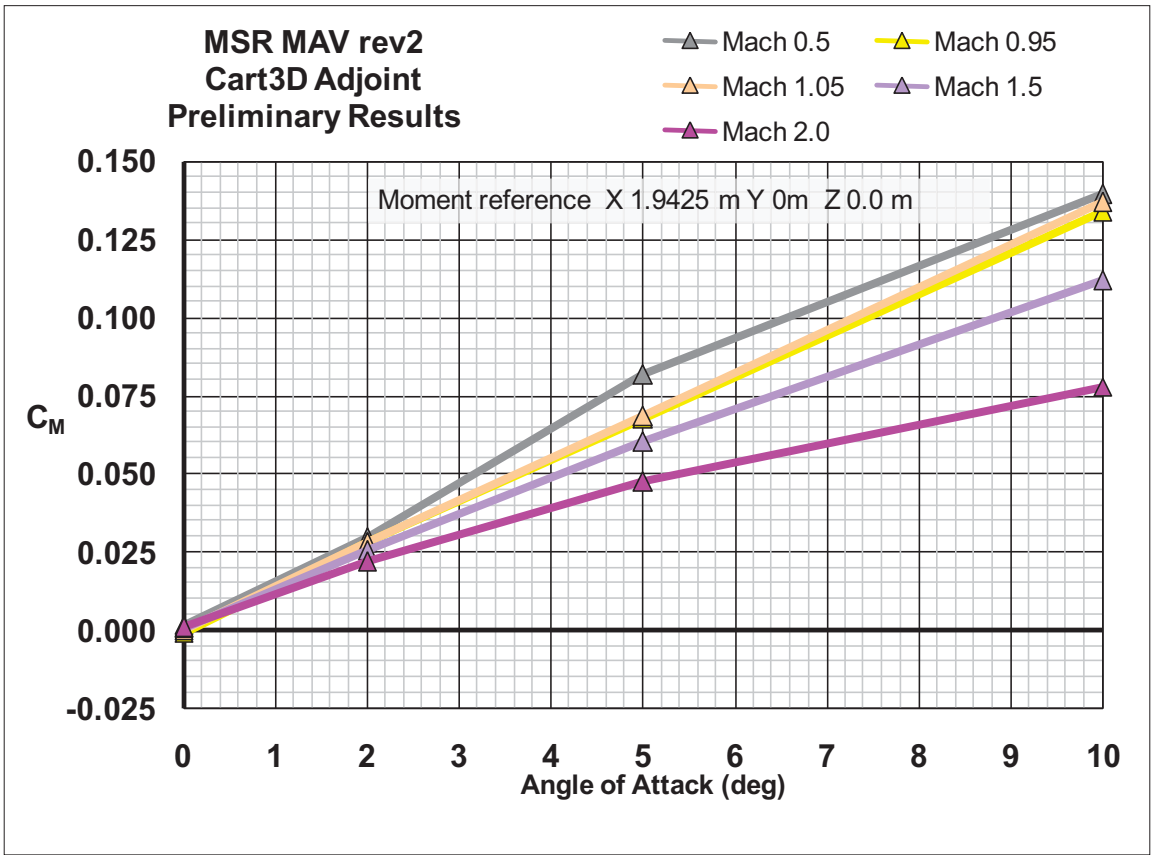


Figure C7. Cart3D predicted pitching moment coefficient versus angle-of-attack and Mach number contours for the Rev2 geometry

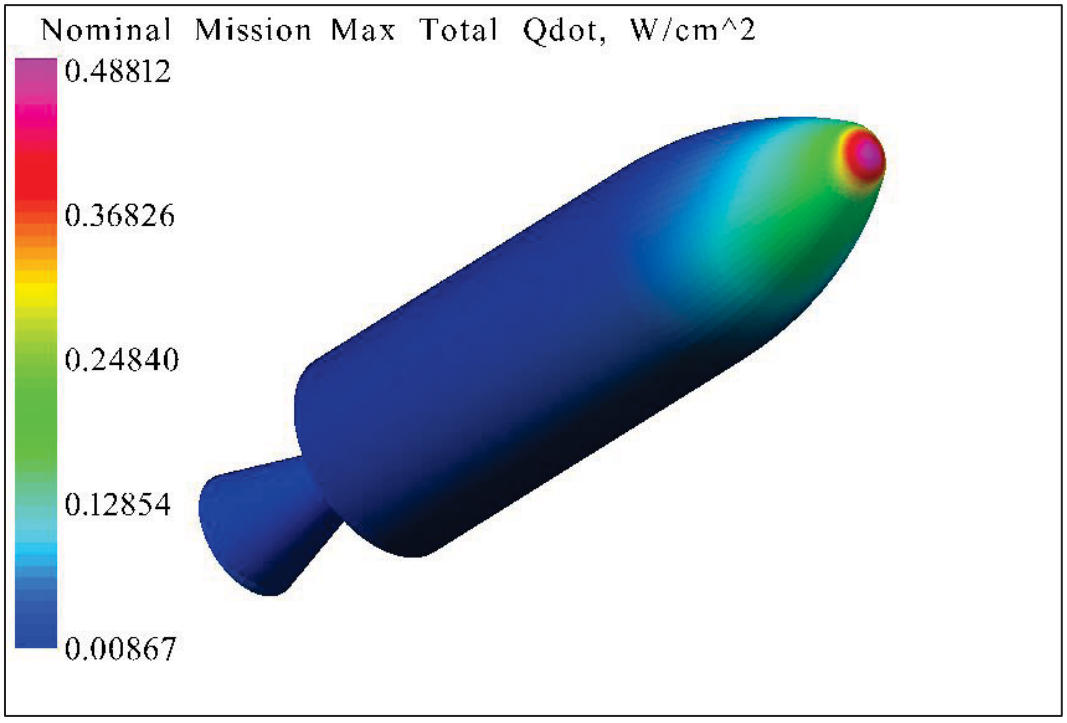


Figure C8. Mission maximum convective heating distribution for Rev2 geometry

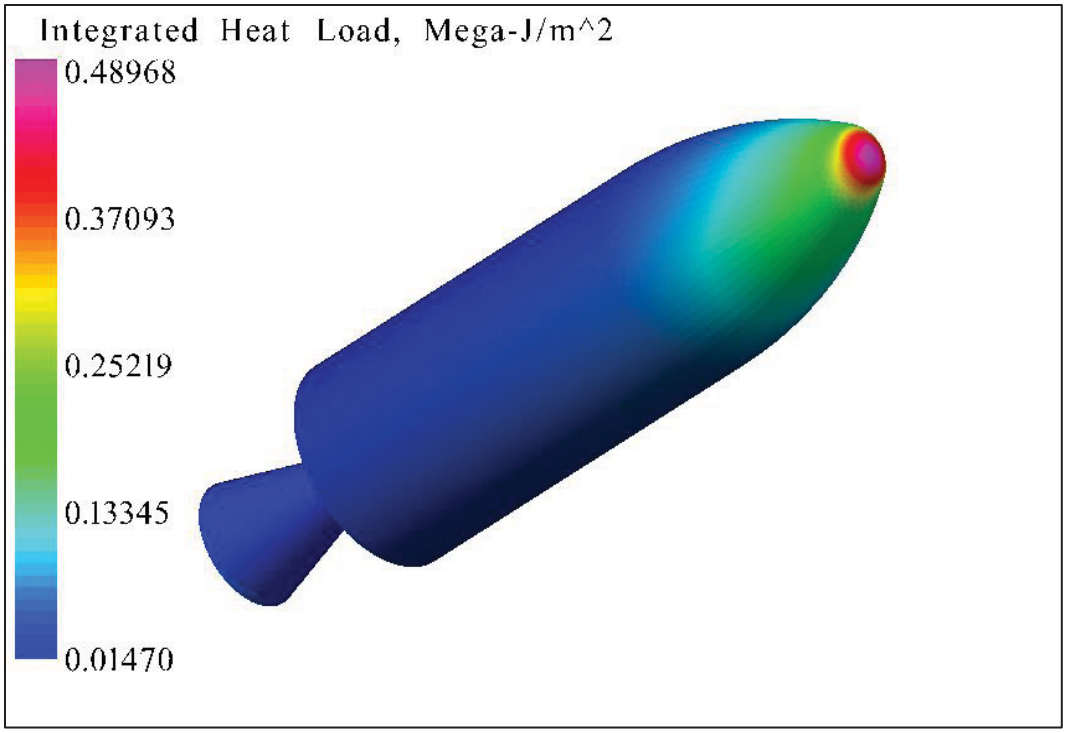


Figure C9. Mission integrated heat load for Rev2 geometry

References

1) Kinney, D.J., “Aero-Thermodynamics for Conceptual Design”, AIAA Paper 13382, January 2004, Reno Nevada

2) Kinney, D. “Aerothermal Anchoring of CBAERO Using High Fidelity CFD”, AIAA Paper 2007-608, January 2007

3) Cart3D documentation website http://people.nas.nasa.gov/!aftosmis/cart3d/

4) Lynn, Emory, “Integrated Rocket Sizing Program”, Version 4.2, User’s Manual, Oct. 2007.

5) Forbos, J. C. and Woodhead, G. E., “Conceptual Design ad Analysis of Hypervelocity Aerospace Vehicles”, Mass Properties, AFWAL Report WL-TR-91-6003, Vol I, Part I.

6) Bowles, J. V. “Conceptual Studies Activities”, Proceedings of the Second National Aerospace Plane Symposium, Applied Physics Laboratory, Laurel MD, Nov. 1986.

7) Whitehead, J. “Propulsion Engineering Study for small-Scale Mars Missions, Lawrence Livermore National Laboratory, UCRL-CR-122442, Sept. 1995.

8) Whitehead, Pittenger, and Colella, “design and Flight Testing of a Reciprocating Pump Feed Rocket, AIAA 94-3032, July 2994

9) G.L. Brauer, et al, “Capabilities and Applications of the program to Optimize Simulated Trajectories (POST),” NASA CR-2770, February 1977.

10) McBride, B. J. and Gordon, S., "Computer Program for Calculation of Complex Chemical Equilibrium Compositions and Applications II. User's Manual and Program Description", NASA RP-1311-P2, June 1996